UNIVERSIDAD DE CANTABRIA

Facultad de Ciencias

Síntesis y caracterización de un nuevo Líquido Iónico Magnético basado en bis(1,3-dimetilimidazolio) μ-oxo bis[tribromoferrato(III)]

(Synthesis and Characterization of a new Magnetic Ionic Liquid based on bis(1,3-dimethylimidazolium) μ-oxo bis[tribromoferrate(III)])

Trabajo de Fin de Grado
para acceder al

GRADO EN FÍSICA

Autor: Palmerina González Izquierdo

Director: Dr. Manuel de Pedro del Valle

Co-Director: Dr. Oscar Fabelo Rosa

Julio - 2016

Acknowledgments

I would like to express my very great appreciation to my advisor Dr. Manuel de Pedro del Valle for his valuable suggestions and motivation during this project. My special thanks are extended to Prof. Jesús Rodríguez Fernández and the entire CITIMAC department for making possible my stay at Institut Laue-Langevin, where I enjoyed and learned so much.

I would like to thank this institution as well for embracing me as a trainee student, allowing me to live this wonderful experience. I am particularly grateful for the patience and helpful explanations of my supervisor at ILL, Dr. Oscar Fabelo, with whom it was a pleasure sharing the office with.

Por último, pero no menos importante, gracias a mis padres. Gracias por vuestros consejos, por apoyarme y creer siempre en mí más que yo misma. Teníais razón en todo.

Resumen

Los líquidos iónicos magnéticos han despertado gran interés en la comunidad científica durante las últimas dos décadas debido a sus interesantes propiedades y posibles futuras aplicaciones. El objetivo de este proyecto es sintetizar y estudiar diferentes tipos de líquidos iónicos magnéticos, centrando el análisis en el nuevo compuesto bis(1,3-dimetilimidazolio) μ-oxo bis[tribromoferrato(III)]. Para esto, se emplearon diversas técnicas experimentales y rutas sintéticas en diferentes centros de investigación para producir y caracterizar estos MILs, por mencionar algunas de ellas: difracción de rayos X en monocristal y radiación sincrotrón en polvo, espectroscopía FTIR y Raman, calorimetría diferencial de barrido, medidas magnéticas en PPMS, etc. Los MILs estudiados durante este proyecto están compuestos de diferentes moléculas de imidazolio y FeX_3, donde X indica el halógeno Cl o Br. La presente memoria detalla las técnicas experimentales utilizadas, así como los resultados obtenidos y su análisis para el compuesto central, además de un resumen de la producción y propiedades destacadas de los demás MILs sintetizados.

Abstract

Ionic magnetic liquids have provoked great interest in the scientific community over the past two decades due to their interesting properties and possible future applications. This project aims to synthesize and study different kinds of Ionic Magnetic Liquids, focusing in a new dinuclear MIL: bis(1,3-dimethylimidazolium) μ-oxo bis[tribromoferrate(III)]. For this purpose, a great variety of experimental techniques were employed to produce and characterize these MILS. These techniques include, to mention a few, single crystal and synchrotron X-ray diffraction, infrared and raman spectroscopy, differential scanning calorimetry, magnetic measurements in a PPMS, etc. The MILs studied are composed by different imidazolium molecules and FeX_3, where the X stands for the halogen Br or Cl. The present report details the implemented procedures together with the results obtained for the main compound, as well as a summary of the production and most significant properties of the other synthesized MILs.

Contents

CHAPTER 1

Introduction

One of the main goals of Materials Science is to develop and study the properties of new compounds. From this point of view, organic-inorganic hybrid systems result really interesting not only for their significance as new materials but also for their numerous possible industrial applications, as they combine characteristics from both organic and inorganic components. Ionic Liquids (ILs) are defined as salts with a melting point lower than 100° C. They are composed by an organic cation, generally imidazolium, pyrrolidinium, pyridinium, etc. and an inorganic anion, like Cl^-, Br^-, I^-, $FeCl_4^-$, $FeBr_4^-$, PF_6^-, etc, bonded by Van der Waals forces. They have gained a tremendous interest in both academia and industry over the past two decades due to their unusual and unique properties, like neglectable vapor pressure, high electric conductivity, thermal stability, etc. [1]

Magnetic ionic liquids (MILs) have received considerable attention among ionic liquids (ILs), fuelled by the possibility of tuning the materials properties by means of external magnetic fields or using them in the liquid state to produce nanoparticle-free magnetic emulsions and micro-emulsions. Moreover, they can combine magnetic and ILs' properties with additional intrinsic thermochromic, magneto-electrochromic or luminescent properties depending on the enclosed paramagnetic ion used. Thus, reports on the synthesis, study and application of these smart materials has proliferated over the past ten years.

1.1 State of the art

In 2004, a magnetic response from an ionic liquid (based on an iron anion [$FeCl_4^-$] and the organic cation 1-buthyl-3-methylimidazolium) was observed in the presence of a neodymium magnet of 0.55 T at room temperature [2]. This was the first Ionic Magnetic Liquid under scrutiny. These earliest compounds developed since their discovery by the group of Hayashi contained a metal anion (such as iron, copper, manganese) and an organic cation, typically imidazolium, pyrrolidinium, pyridinium, etc. Currently, the combinations of different rare-earth (europium, neodymium, dysprosium, etc.) chiral amino-acids, dicationic ions tricationic ions or heteroanions, etc, have been studied for application in transport and separation of materials, [3] separation of greenhouse gases (CO_2) through supported magnetic ionic liquid membranes, [4] magnetic surfactants, [5] extraction of DNA, [6] or esterication of oleic acid to biodiesel. [7]

This project follows the same research line than previous studies taking place at University of Cantabria (ref. [8]). This doctoral thesis is a corollary of different publications in well-known scientific journals about five new different imidazolium-based MILs, being the metal complex ion a three-coordinated iron atom with halogen elements (Cl and Br) (these compounds are shown in Fig. 1.1). All these complexes are mononuclear, meaning that there is only one Fe atom per inorganic molecule, and were used as precursors in order to obtain new MILs during this project. The compound in which this present report is focused is a dinuclear MIL (two irons joined by an oxo-bridge in the inorganic molecule) obtained from the precursor 1,3-dimethylimidazolium tetrabromoferrate(III) (Fig. 1.1b, bottom). Even though these kind of dinuclear MILs have been already reported in numerous studies, [9–12], all the research is focused generally in chloro-based compounds, being very scarce in bromide complexes. [13, 14] Appart from trying to obtain dinuclear units instead of mononuclear ones, the other novelty in the present report is the utilization of a different imidazolium molecule (1,2,3-trimethylimidazolium, shown in Fig. 1.2c) in order to synthesize new MILs, which has also scant appearance in scientific publications.

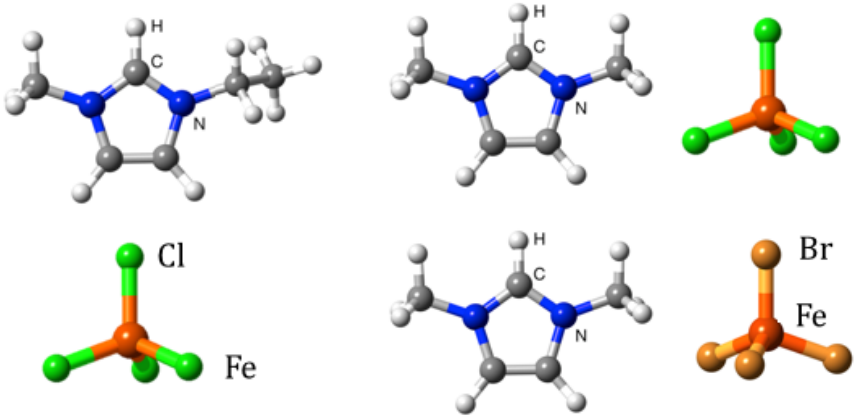

(a) Emim[$FeCl_4$] (b) Dimim[FeX_4]

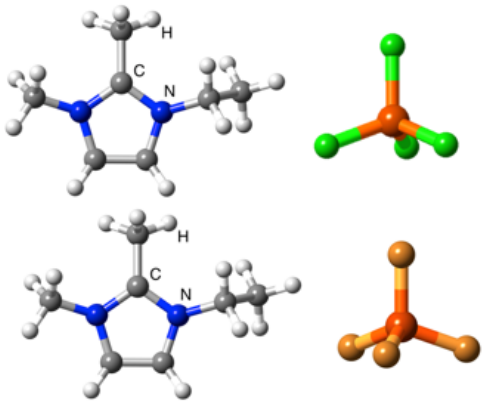

(c) Edimim[FeX_4]

Figure 1.1: Synthesized mononuclear MILs in Ref. [8]. X stands for Cl and Br.

The results presented in this report will be compared to those in Ref. [8] together with other related scientific publications. The main conclusions extracted from the study of the MILs that are shown in Fig. 1.1 can be summarized as follows:

- These compounds are structured in layers of organic and inorganic ions pillared along the b-axis.
- They all present long-range antiferromagnetic ordering at low temperatures.

- The Néel temperature is influenced by the electronic transfer from the metal to the halogen together with the overlapping of the orbitals. For this reason, the ordering temperature increases in the case of Br respect to the chloride complexes, as the former bonding is more covalent than the latter. Unlikely, it was found that the size of the imidazolium molecule is not the main factor which affects to the strength of magnetic interactions (T_N was higher for Edimim than for Dimim).

The method performed to synthesize these magnetic ionic liquids from Ref. [8] is detailed below.

1.1.1 Production of mononuclear MILs

The most common way to obtain these MILs consists in a solid-solid reaction under inert atmosphere before thermal heating at moderate temperatures. [15] The most complex step is to obtain the starting organic salts, due to the fact that most of them are not commercial and depending on their purity or complexity, they might need some preliminary steps, increasing their price considerably. The organic salts employed to synthesize the precursor MILs appearing in this report are 1,3-dimethylimidazolium (Dimim$^+$), 1-ethyl-2,3-dimethylimidazolium (Edimim$^+$) and 1,2,3-trimethylimidazolium (Trimim$^+$). These organic molecules are shown in Fig. 1.2.

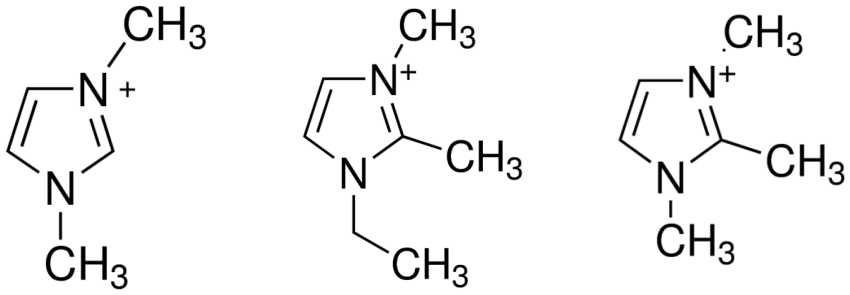

(a) Dimim$^+$ (b) Edimim$^+$ (c) Trimim$^+$

Figure 1.2: Starting organic cations employed in this report.

CHAPTER 2

Experimental section

2.1 Synthesis Overview

Even though this report will be focused on the study of the new dinuclear MIL $Dimim_2[Fe_2OBr_6]$ (named compound (**1**) hereafter) synthesized during this project (detailed in section 2.1.3), numerous compounds were produced and examined. This research is out of the scope of this proposal, but some of the performed techniques and analysis will be described briefly.

2.1.1 Precursors

During this project, different synthesis techniques were approached in order to obtain new MILs. The precursors utilized were in some cases mononuclear MILs already synthesized, dinuclear MILs also already produced or the starting organic and inorganic salts from scratch. In this section, the synthetic routes to obtain these precursors will be detailed, while those performed from them in order to obtain MILs will be described in section 2.1.2.

- The Dimim[$FeBr_4$] and Dimim[$FeCl_4$] precursors were freshly obtained through a thermal treatment inside a glove-box as described in section 1.1.1 [1]. [16, 17]
- 1,3-dimethylimidazolium chloride (Dimim[Cl]) was purchased from commercial sources and used without further purification.

[1] A detailed description of the synthetic routes can be consulted in Ref. [8].

- Synthesis of 1-ethyl-2,3-dimethylimidazolium bromide (Edimim[Br]): 1,2- dimethylimidazole (9.38 g, 97.5 mmol) was dissolved in 150 ml acetonitrile and ethyl iodide (11.68 g, 107.25 mmol) was added dropwise to the stirred solution cooled in an ice bath. After addition of the iodometane, the reaction mixture was warmed up and the mixture refluxed for 24h. The reaction was cooled down and the solvent removed under vacuum. The remaining solids were re-crystallized in a mixture of acetone: acetonitrile yielding white crystals 15.80 g, 79% yield.

- 1,2,3-trimethylimidazolium iodide (5 g, 19.84 mmol) was dissolved in 500 ml of distilled water and passed through an anion exchange column Amberlite IRA-400 column (OH- form) to yield a iodide free solution of 1,2,3- dimethylimidazolium hydroxide (test by the Volhard method). The hydroxide solution was neutralized with concentrated hydrobromic acid (36%, Vetec) to pH 7 and water removed in rotary evaporator with the remaining water removed under vacuum at 100º C. The solids were then dissolved in dichloromethane and dried over anhydrous Na_2CO_3, filtered and the solvent removed under vacuum, yielding 4.80 g (96%) of l,2,3-trimethylimidazolium bromide (Trimim[Br]).

- 1-ethyl-2,3- dimethylimidazolium Heptachloridoferrate (III) (Edimim $[Fe_2Cl_7]$): In a glove-box, the 1-ethyl-2,3- dimethylimidazolium chloride (1 g, 4.90 mmol) was mixed with anhydrous $FeCl_3$ (1.6 g, 9.80 mmol) in a 8 ml vial. The mixture was heated at 100ºC and the desired 1,3-dimethylimidazolium Heptachloridoferrate product was obtained as a red solid., 2.6 g (100% yield).

2.1.2 Synthetic Procedures

During this project, a lot of synthetic procedures have been performed in order to obtain more dinuclear MILs or recrystallize those already produced. The main difference between the mononuclear and dinuclear MILs is that the former were obtained as powder and the latter as crystals (usually needle-shaped). The synthetic routes approached to achieve these aims are summarized below:

- **Dimim$_2$[Fe$_2$OBr$_6$]** (0.176 g, 0.21 mmol) was dissolved in 10 ml of 2-Propanol (compound (**2**)) and in 13 ml of 1-Heptanol (compound (**3**)). The solutions were stirred and heated up to 75ºC approx. and cooled slowly until RT (Room Temperature) after one hour. The resulting dark-red crystals (58 mg, 34% yield) were separated from the mother-liquor and washed with hexane. IR and DSC measurements suggest

that the resulting products are not dinuclear and are different compounds from the precursor. A picture of the resulting crystals from the 2-Propanol recrystallization is shown in Fig. 2.1a.

- Recrystallization of **Edimim**[$\mathbf{Fe_2Cl_7}$][2]
  - Recrystallization in 2-Propanol (0.117 g, 0.24 mmol in 10 ml) and 1-Heptanol (0.117 g, 0.24 mmol in 13 ml). The procedure was similar in both cases: the solutions were stirred and heated up during 1.5 hours to 100°C and 82°C, respectively, and slowly cooled until RT. In both cases, a dark-brown dust is obtained (30 mg, 26% yield in the case of the 2-Propanol and 69 mg, 59% yield in the case of the 1-Heptanol), which is separated from the mother liquor and washed with hexane.
  - Recrystallization in mixture of Methanol and 1-Heptanol (0.117 g, 0.24 mmol in 4 and 15 ml, respectively). There was no need of warming up in this last procedure, as the reactive was highly soluble in Methanol. After stirring until all the reactive is solved, the solution is filtered at 45 μm. After two days evaporating, 38 mg (32% yield) of yellow needles precipitate (0.5 cm long approx).

- **Edimim**[$\mathbf{FeCl_4}$] was dissolved in 2-Propanol while stirring and heating up. The product of that reaction was recrystallized via different routes.
  - Recrystallization in 1-Heptanol (0.081 g, 0.25 mmol in 15 ml). The solution was stirred and heated up to 90°C approx and cooled slowly until RT after 1.5 hours. The resulting brown dust was separated from the mother-liquor and washed with hexane (16 mg, 20% yield).
  - Recrystallization in mixture of Methanol and 1-Heptanol. Heating up was not necessary as the mono-nuclear MIL is very soluble in Methanol. Two similar synthesis were carried on, the first one (0.081 g, 0.25 mmol in 1 ml MeOH and 15 ml HepOH) resulted in small yellow needles (36 mg, 44% yield) with a small percentage of brown dust after 3 hours. The second one (0.081 g, 0.25 mmol in 4 ml MeOH and 15 ml HepOH) was filtered at 45 μm and allowed to evaporate more slowly, which resulted also in small yellow needles (55 mg, 68% yield). The products of both synthesis were separated from the mother-liquor and washed with hexane.

[2]It is thought to be a dimer, but future X-Ray diffraction is needed to solve its structure.

- Recrystallization of **Dimim[$FeCl_4$]**
  - The precursor was dissolved in 5 ml of 1-Heptanol (0.074 g, 0.25 mmol) after heating up to 60º C for 45 min approx. 44 mg (59% yield) of yellow needles were obtained after cooling to RT and allowing it to evaporate, which were separated from the mother-liquor and washed with hexane.
  - The precursor and $FeCl_3$ was dissolved stoichiometrically (0,74 g, 0.25 mmol Dimim[$FeCl_4$] + 0.041 g, 0.25 mmol $FeCl_3$) in 13 ml of 1-Heptanol. The solution was stirred and heated up to 88º C for 20 min approx. After letting it cool down to RT and evaporate for 2 days, 64 mg (56% yield) of yellow needles were precipitated. This crystals were separated from the mother liquor and washed with hexane.
  - The precursor (0.074 g, 0.25 mmol) was dissolved in a mixture of Methanol and 1-Heptanol. Two similar synthesis were carried out, resulting both of them in yellow needles. The first one (0.074 g, 0.25 mmol in 1 ml MeOH and 15 ml HepOH) was evaporated faster (3 hours) than the second one (0.074 g, 0.25 mmol in 4 ml MeOH and 15 ml HepOH). The quality and the yield of the product of the slowest crystallization was higher (35 mg, 47% yield in comparison to 23 mg, 31% yield), giving rise to bigger needles (1 cm long approx.).

- Synthesis of **Trimim[Br] + $FeBr_3$:** solid-solid reaction under inert atmosphere, as explained in section 1.1.1. After mixing both reactives stoichiometrically (0.048 g, 0.25 mmol Trimim[Br] + 0.074 g, 0.25 mmol $FeBr_3$), they were taken out of the glove-box and dissolved in a mixture of Methanol and 1-Heptanol right after (8 ml and 10 ml, respectively). This process has to be performed rapidly to avoid the contact with air due to the fact that both reactives are highly hygroscopic. After stirring until it is completely dissolved, the dark-red solution is filtered at 45 μm. After slowly evaporating for one week, 48 mg (39% yield) of dark-red plate-like crystals precipitate (see Fig. 2.1b). They were separated from the mother liquor and washed with hexane.

- Synthesis of **Edimim[Br] + $FeBr_3$:** solid-solid reaction under inert atmosphere, as explained in section 1.1.1. Two different routes were carried out stoichiometrically:

  - 1 Edimim[Br] + 1 $FeBr_3$ (0.82 g, 4 mmol + 1.18 g, 4 mmol). After mixing the reactives, the misture was heated in an oil bath up to 130º C for 1.5 hours, resulting in a dark-red compound (not completely liquid). After cooling it down to RT, the product was recrystallized in Methanol (0.125 g, 0.25 mmol in 20 ml), Ethanol (0.075 g, 0.15 mmol in 50 ml) and in mixture of Methanol and Heptanol (0.125 g, 0.25 mmol in 12 and 20 ml, respectively)[3]. A dark-red solution was obtained in the three synthetic routes. After dissolving completely, they were filtered at 45 μm and allowed to evaporate slowly (55 mg, 44% yield).
  - 1 Edimim[Br] + 2 $FeBr_3$ (0.413 g, 2.02 mmol + 1.19 g, 4.04 mmol). After mixing the reactives, the mixture was heated in an oil bath up to 130º C for 1.5 hours, resulting in a dark-red compound (not completely liquid). After letting them cool down to RT, the compound with the same number or organic and inorganic molecules was heated up again to 130º C while open. This was done in order to oxydate the sample (to create the oxo-bride Fe-O-Fe). This procedure was not carried out with the other synthesized compound, as it was more likely to produce dimers of the type Edimim[Fe_2Br_7] rather than $Edimim_2[Fe_2OBr_6]$. IR spectrum suggests the absence of this O-Fe bond, which indicates that it is the mononuclear MIL Edimim[Br].

- Synthesis of **Dimim[Cl] + $FeCl_3$:** this time, instead of the typical solid-solid reaction, the organic salt (0.066 g, 0.5 mmol) was dissolved in in 60 ml of Ethanol before adding the $FeCl_3$ (0.081 g, 0.5 mmol). The reactives were rapidly dissolved, resulting in a yellow solution. This solution was left stirring in contact with air for several days[4].

[3]The molecular weight used was that of the monomer Edimim[$FeBr_4$]
[4]Similar to the synthesis carried out by Jui-Cheng Chang *et al.* (Ref. [12]).

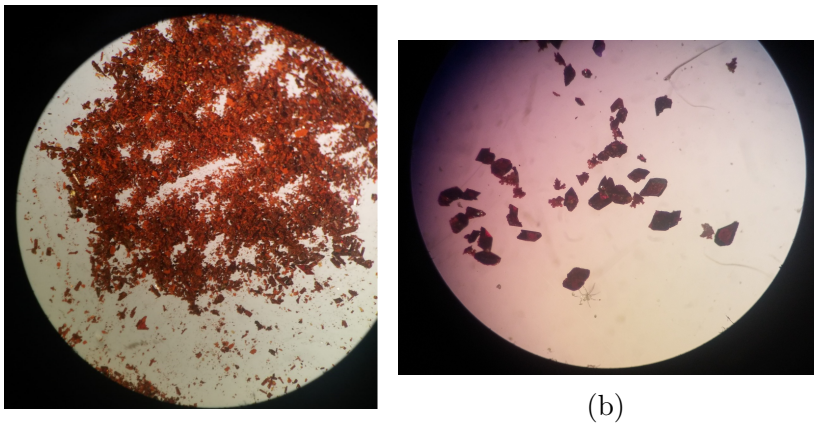

(a) (b)

Figure 2.1: Two resulting brominated crystals seen under a magnifying lens. Recrystallization of compound(**1**) in 2-PrOH (a) and Trimim[Br] + $FeBr_3$ in MeOH and HepOH (b).

2.1.3 Synthesis of Dimim$_2$[Fe$_2$OBr$_6$]

(**1**). A 2-propanol solution (15 ml) was added to the freshly prepared Dimim [$FeBr_4$] precursor (0.118 g, 0.25 mmol). The solution was heated at 70º C and vigorously stirred during 45 min. After this time, it was allowed to cool down to RT. The dark brown solution was stored at room temperature. After 24 hours, a small plate-like dark-red single crystals suitable for single crystal X-ray diffraction were obtained. They were separated from the mother-liquor and washed with hexane.

2.2 Physical characterization techniques

2.2.1 Single-crystal X-Ray Diffraction

Single crystal X-ray diffraction data was collected at 100(2) K using an Agilent Technologies Supernova diffractometer equipped with Molybdenum micro-source (0.71073 Å) at UPV/EHU, Bilbao. The data were indexed, integrated and scaled with the CrysAlisPRO program. [18] The crystal structure was solved by direct methods and refined with the full-matrix least-squares technique on F^2 by using the SHELXS-97 and SHELXL-97 programs, respectively, [19] included in the WINGX software package. [20] Anisotropic thermal parameters were used to refine all non-hydrogen atoms. The hydrogen atoms of the 1,3-dimethylimidazolium molecule were found in

the difference Fourier map and isotropically refined without restrains. The final geometrical calculations and the graphical manipulations were carried out with the DIAMOND program. [21] A summary of the crystal data and refinement conditions is listed in Table 2.1.

Formula	C_{10} H_{18} Br_6 Fe_2 N_4 O
Formula weight	801.44
Crystal system	Monoclinic
Space group	C $2/c$
a (Å)	16.7749(6)
b (Å)	7.5979(3)
c (Å)	18.2318(8)
α (°)	90
β (°)	105.187(4)
γ (°)	90
V (A^3)	2242.56(16)
Z	4
μ (cm^{-1})	11.989
T (K)	293(2)
ρ_{calcd} (g cm^{-3})	2.374
λ (Å)	0.71073
index ranges	$-11 < h < 22$
	$-8 < k < 10$
	$-23 < l < 22$
total reflns	8187
indep. reflns (R_{int})	2549
obsd reflns [$I > 2\sigma(I)$]	2231
parameters	138
GOF	1.053
R [$I > 2\sigma(I)$]	0.0321
R_w [$I > 2\sigma(I)$]	0.0719
R [all data]	0.0386
R_w [all data]	0.0755

Table 2.1: Crystal data and details of the structure determination for complex (**1**).

The fundamentals of X-ray diffraction and the procedure to solve the crystal structure from the data (Rietveld method) are detailed in appendix A.

2.2.2 Synchrotron Diffraction

The entire world of synchrotron science depends on one physical phenomenon: when a moving electron changes direction, it emits energy (the so-called synchrotron radiation). When the electron is moving fast enough, the emitted energy is at X-ray wavelength.

A synchrotron machine exists to accelerate electrons to extremely high energy and then make them change direction periodically. The resulting X-rays are emitted as dozens of thin beams, each one directed toward a beamline next to the accelerator. The X-rays coming from these large synchrotron facilities have two great advantages over the "home-made" X-rays. First of all, as they produce a wide wavelength range from microwaves to X-rays, the desired wavelength can be selected and it is highly collimated (which is translated into an increase in resolution) and secondly, its bright (magnitude related to the intensity) is several orders of magnitude higher.

The synchrotron diffraction patterns shown in this report were measured at ALBA Synchrotron, in Barcelona, selecting a wavelength λ =0.61937 Å. The diffraction patterns were aquired at 300 K, 100 K, 300 K, 350 K and 300 K, following that order.

2.2.3 FTIR Spectroscopy

Fourier transform infrared spectroscopy (FTIR) is a technique used to obtain an infrared spectrum of absorption or emission of a solid, liquid or gas. In a molecule, the bonds between the atoms are not static and are free to vibrate, either stretching (change in the length of a bond) or bending (change in the angle of a bond). Both types of vibrations represent different energy levels of a molecule and the difference between them lies on the infrared range. Because each different material is a unique combination of atoms, no two compounds produce the exact same infrared spectrum. Therefore, infrared spectroscopy can result in a positive identification (qualitative analysis) of every different kind of material. In addition, the size of the bands in the spectrum is a direct indication of the amount of material present.

The classical and most straightforward way to obtain the IR spectra is using the so-called dispersive spectrometers. These devices project a unique monochromatic light beam and measure how much of it arrives to the detector for each wavelength (which is changed after each measurement by a grating). Fourier transform spectroscopy is a less intuitive method to obtain the same information. Rather than shining a monochromatic beam of light at the sample, this technique shines a beam containing many frequen-

cies of light at once and measures how much of that beam is absorbed by the sample. Next, the beam is modified to contain a different combination of frequencies, giving a second data point. This process is repeated many times. Afterwards, a computer takes all these data and works backwards to infer what the absorption is at each wavelength. This can be accomplished by the use of an interferometer and a well-known mathematical technique called the Fourier transformation. The interferometer consists basically in a beam splitter and two mirrors, one of them static and the other one moving. The beam is splitted in two beams and directed to the mirrors. The reflected beams are then recombined to form an interference pattern, called interferogram. This interferogram posses the unique property that every data point (a function of the moving mirror position) which makes up the signal has information about every infrared frequency which comes from the source. Finally, the computer performs the Fourier transformations and presents the user with the desired spectral information for analysis.

Measurements were performed in a FT/IR-4600 (Jasco) spectrophotometer in the 400–4000 cm^{-1} range, at Institut Laue-Langevin, Grenoble. This device covers a wavelength range from 350 to 7.800 cm^{-1} with a resolution of 0.7 cm^{-1}. It counts with a 45º Michelson interferometer with aluminum coated mirrors and a Ge/KBr beam splitter. The IR beam is generated by a high-intensity ceramic source and detected by a DLATGS (Deuterated Lanthanum-Alanine doped TriGlycine Sulphate), which is a pyroelectric detector.

2.2.4 Raman Spectroscopy

This technique is complementary to the aforementioned FTIR spectroscopy. It is based on inelastic or Raman scattering, in which the frequency of the incoming light is shifted due to the vibrations of a system. Therefore, when a monochromatic beam passes through a material (usually from a laser in the visible, near infrared or near ultraviolet range), it interacts with molecular vibrations, phonons or other excitation in the system, thus producing a very intense peak corresponding to the elastic or Rayleight scattering, and highly weaker peaks due to the Raman scattering. These peaks appear in pairs and are symmetric respect to the Rayleight frequency. Those with lower energy correspond to the Stokes Raman scattering, where the material absorbs energy, and those with higher frequency are due to the increase in energy of the emitted photon and is known as anti-Stokes scattering. This technique provides a fingerprint of each material in the same way than for FTIR.

The basic scheme of a Raman spectrophotometer is shown in Fig. 2.2. The bare functioning of these devices is rather simple. It counts with two filters: a laser line filter for selecting the wavelength of the incident light and blocking all the others and a notch filter for blocking only the laser line while passing both long and shorter wavelengths. The light from the laser, then, passes through the laser line filter to ensure that is highly monochromatic, it scatters while traversing the sample and the notch filter blocks the Rayleight wavelength, letting all the other frequencies to reach the spectrometer, which measures the intensity for each one of them. This procedure allows us to measure both Stokes and Anti-Stokes Raman scattering simultaneously.

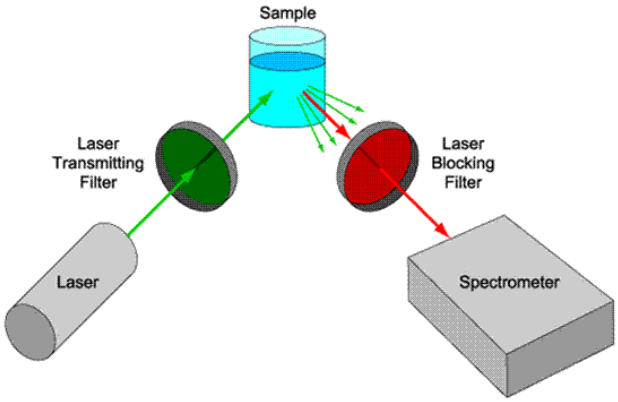

Figure 2.2: Sketch of a Raman spectrophotometer.

The room-temperature nonpolarized Raman spectra were obtained in the backscattering geometry with a Horiba T64000 triple spectrometer with a confocal microscope in the single mode equipped with an edge filter that had a resolution of 1 cm^{-1}, a 1800 grooves/mm grating and a 100 μm slit and was equipped with a liquid N_2-cooled CCD detector (Jobin-Yvon Symphony). A 514.5 nm line of a Coherent Innova Spectrum 70C Ar^+-Kr^+ laser was focused down with a 20$\times$ objective. The power on the sample was kept below 5 mW to avoid laserheating effects on the probed material and the concomitant softening of the observed Raman peaks.

2.2.5 Differential Scanning Calorimetry

The Differential Scanning Calorimetry or DSC is a simple technique which consists in measuring the difference in heat flow transmitted to a sample respect to a reference for them to remain at the same temperature. Generally, the temperature program for a DSC analysis is designed such that

the sample holder temperature increases linearly as a function of time. The reference sample should have a well-defined heat capacity over the range of temperatures to be scanned.

It is known that during phase transitions, the temperature does not change, unlike the heat flow, which increases or diminishes depending if it is an endothermic or an exothermic process. Therefore, this technique allows us to see the different phase transitions occurring in a compound by measuring the variation in the heat flow respect to the reference.

Measurements were performed in a DSC131 (Setaram) device at Institut Laue-Langevin, Grenoble, in a temperature range 25-150C.

2.2.6 Magnetic Susceptibility measurements

Needless to say that measuring the magnetic response of the compounds could not be left out of this project, being studying magnetic ionic liquids. In this section, the magnetization of the sample under different magnetic fields and temperatures was measured in order to elucidate its magnetic nature. From the magnetization $\vec{M}$, it is possible to obtain the molar magnetic susceptibility χ_m by knowing the applied field $\vec{H}$ using this expression:

$$\chi_m = \frac{m}{M}\frac{\vec{M}}{\vec{H}} \tag{2.1}$$

Where m is the mass of the sample and M the molar mass.

For acquiring these data, a magnetometer was employed. These devices count with a coil inside a dewar flask which generates a magnetic field. That flask contains liquid Helium and is placed inside a bigger one full of liquid Nitrogen for the He consumption to be minimum and the isolation, maximum.

The sample with known mass is placed in a small plastic polymeric capsule which is previously calibrated in the same temperature range and magnetic field that will be used later for the proper measurements. Once the sample is fixed in the plastic tube, the chamber is under vacuum and filled with He gas, the measurement process can start. When a current circulates through the coil it generates a magnetic field, according to Faraday's law, which will interact with the magnetic moments of the sample, inducing (or not, depending on its magnetic nature) a net magnetization. This magnitude is measured respect to the temperature and the applied field.

Variable-temperature magnetic susceptibility measurements were performed using a standard Quantum Design PPMS (Physical Property Measurement System) magnetometer at CITIMAC, University of Cantabria, whilst heating from 2 to 300 K in the $0.1 \leq H/kOe \leq 80$ range after cooling in either the presence (field cooling, FC) or the absence (zero field cooling, ZFC) of the applied field. Magnetization as a function of field (H) was measured using the same magnetometer in the $-80 \leq H/kOe \leq 80$ range at 2 and 30 K after cooling the sample in zero field.

2.3 Future Measurements

2.3.1 Neutron Diffraction

Although this technique was not employed during this project, it is essential to solve the magnetic structure of the compound. In order to perform this kind of measurements, it is necessary to apply for beam time to large facilities like the Institut Laue Langevin, in Grenoble, which gave us permission to realize this technique in the future (the project proposal can be found attached in appendix C). The principles of Neutron scattering will be introduced below.

Neutron diffraction can be used as a complementary technique to X-Ray diffraction to determine the crystal structure of materials. Although this technique requires more acquisition time than X-ray, the advantage is that neutrons interact directly with the nuclei of the atoms. This fact makes possible to distinguish different isotopes (the number of electrons is the same, thus not being able to distinguish them using X-ray) and determine the position of Hydrogen atoms (which have the lowest scattering power in X-ray diffraction). The other important fact about neutrons is that they are fermions, meaning that they have 1/2 spin, becoming an essential tool to determine the magnetic structure of a sample.

The way of proceeding is the following: two diffraction measurements must be acquired, one above the temperature of magnetic ordering and the other one below it, on such a way that the first one provides uniquely the nuclear structure while the second one posses both, the nuclear together with the magnetic structure. This appears as new peaks in the low temperature diffraction pattern, which can be superimposed to the nuclear peaks or appear

in new positions[5]. The propagation vector $\vec{k}$ can be determined by indexing these satellite peaks and then used to get the basis vectors of the irreducible representations of the propagation vector group. With this information, one can determine the magnetic structure of the crystal by refining again using the Rietveld method with two phases in the crystal, corresponding to the nuclear and the magnetic ones (see append. A).

An example of this procedure is shown in Fig. 2.3. It corresponds to two powder diffraction patterns (the low temperature data and the refinement in the paramagnetic state) of $LaMnO_3$ taken at the LLB diffractometer G4.2 with λ=2.59 Å. The space group is **G**=*Pbnm*, the cell parameters are $a = 5.53$ Å, $b = 5.75$ Å and $c = 7.68$ Å (Ref [22]). These diffraction patterns were refined during the **9^{th} ILL Annual School on Neutron Diffraction Data Treatment using the FullProf Suite**[6]. We can see new peaks below the magnetic ordering temperature ($T_N = 140$ K) in Fig. 2.3 that did not appear in the paramagnetic state. By indexing those peaks it was possible to determine the propagation vector with the help of the software K_Search, which resulted to be $\vec{k} = (0, 0, 0)$ as expected (there are some peaks with both contributions nuclear and magnetic) and then the irreducible representations (*irreps*) with the program BasiReps[7].

Using a trial and error method, the correct *irrep* is found so that the Rietveld refinement can be applied again to solve the final magnetic structure. In this case, the unit cell is the same than the nuclear phase and the Mn atoms' momenta are antiferromagnetically disposed in layers along the *c*-axis (see Fig. 2.4).

[5]The appearance of magnetic peaks in the same position as the nuclear ones is an indicator that the propagation vector is $\vec{k} = (0, 0, 0)$

[6]This course was followed in order to learn how to handle the FullProf Suite package to analyse the neutron diffraction data in the future.

[7]All these programs are contained in the FullProf Suite package.

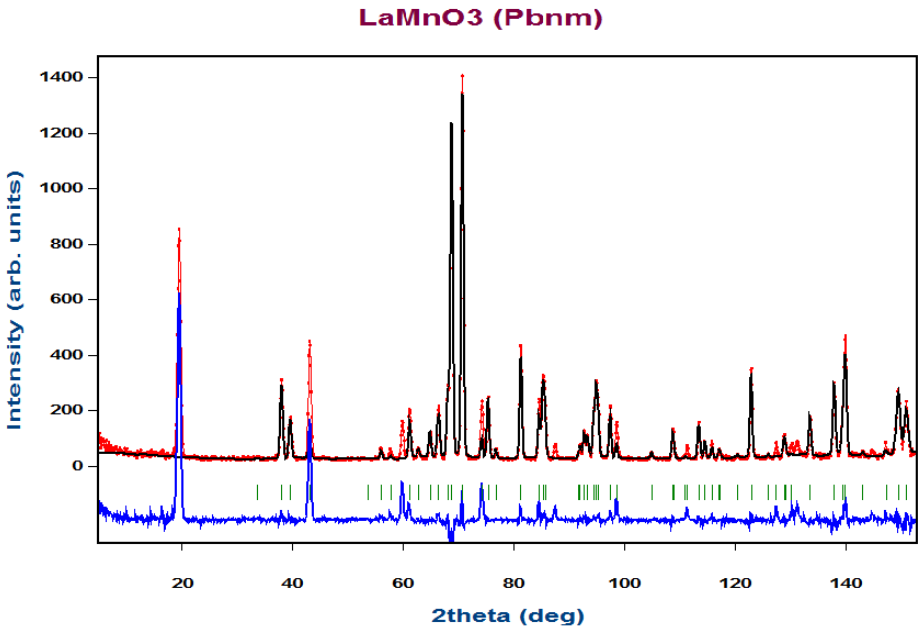

Figure 2.3: Diffraction pattern of $LaMnO_3$ at 50 K (red points) superimposed to the refinement of the nuclear strcuture at 150 K (black solid line). The blue line corresponds to the difference between both patterns.

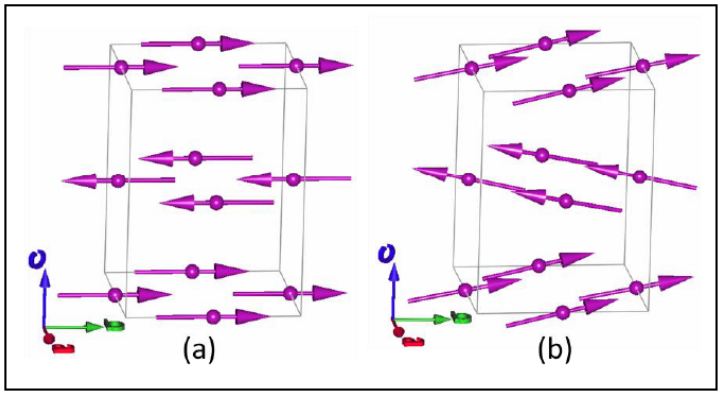

Figure 2.4: Magnetic structure of $LaMnO_3$. Both (a) and (b) arrangements are valid.

2.3.2 X-Ray absorption near edge structure

X-rays are ionizing electromagnetic radiation that have sufficient energy to excite a core electron of an atom to an empty state below the ionization threshold called an excitonic state, or to the continuum which is above the ionization threshold. Different core electrons have distinct binding energies; consequently, if one plots the X-ray absorbance of a specific element as a function of energy, the resulting spectrum will appear similar to Figure 2.5.

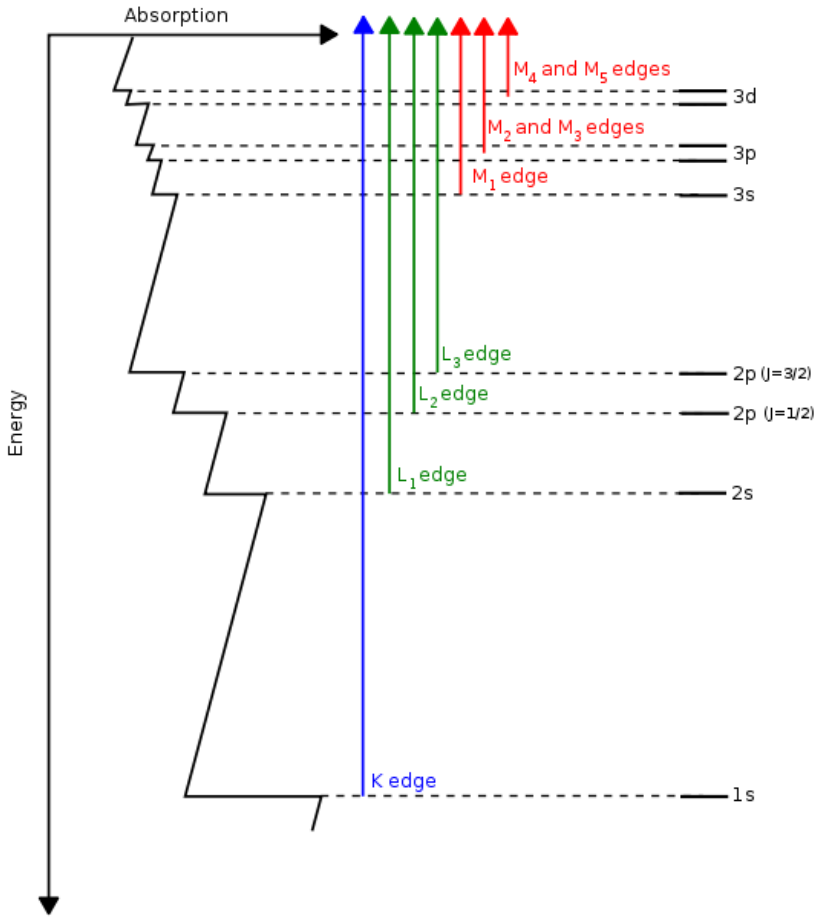

Figure 2.5: Illustrative X-ray absorption spectrum of an transition metal atom. Three major transitions K, L, and M edge transitions are identified, the L edge fine structures are also shown.

As stated above, a core hole is the space a core electron occupied before it absorbed an X-ray photon and was ejected from its core shell. They are created through processes in which either a core electron absorbs an X-ray photon (X-ray absorption) or absorbs part of its kinetic energy (X-ray Raman scattering). This is translated into a sudden increase of absorption of the incoming X-ray beam, which corresponds to a specific type of core-electrons and gives rise to the so-called absorption edge due to its sharp appearance.

X-ray absorption near edge structure measurements or XANES will be performed at Diamond Light Source, in the UK, for the dinuclear and mononuclear MILs in the liquid state to elucidate which metallic species are majority in this phase. The project proposal can be found attached in appendix C.

CHAPTER 3

Results and analysis

3.1 Crystal structure description

The title compound (**1**) $Dimim_2[Fe_2OBr_6]$ is built up from one [Dimim]+ cation and with half of a μ-oxo-bis[tribromoferrate(III)] anion in the asymmetric unit, crystallized in the centrosymmetric monoclinic space group $C2/c$ (No. 15). A detail of the asymmetric unit of (**1**) is presented in Figure 3.1, a list of selected crystallographic information, bond lengths and angles are presented in Tables 3.3, 3.2 and 3.1. The crystal structure can be described as a stacking of organic [Dimim]+ and inorganic $[Fe_2OBr_6]^{2-}$ layers extended in the *ab*-plane and pillared along the *c*-axis, following a *ABCDABCD* sequence similar to that observed on the mononuclear $DimimFeCl_4$ and $DimimFeBr_4$ (see Fig. 3.2). [16, 17]

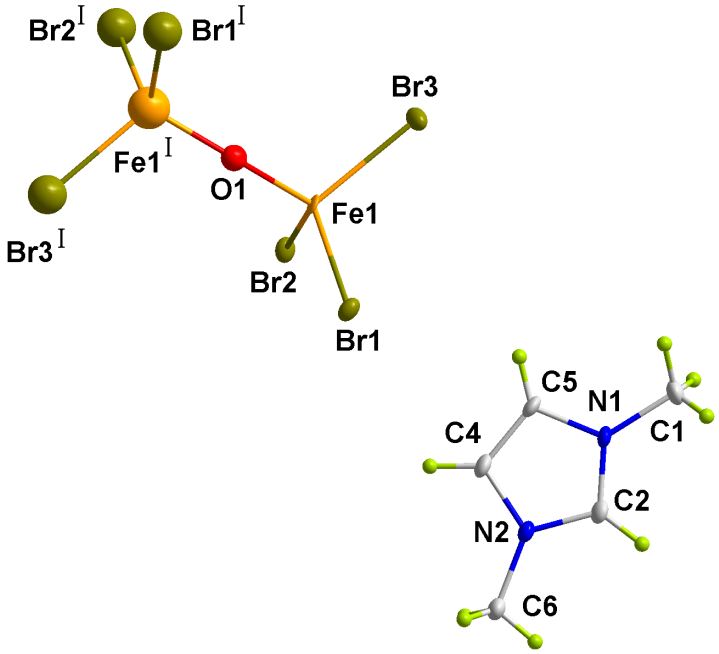

Figure 3.1: Molecular structure of the title compound (**1**). The atoms of the asymmetric unit are shown as displacement ellipsoids, drawn at 50% probability level. H atoms are shown as small spheres of arbitrary radii. [Symmetry code: (I) -x, y, 0.5-z]

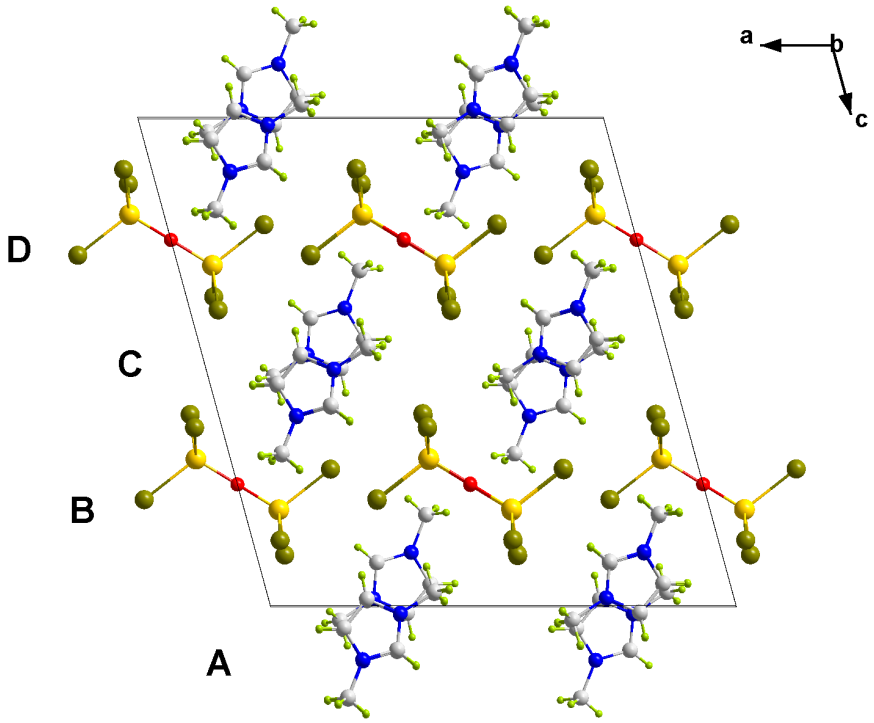

Figure 3.2: Crystal structure of compound (**1**). Iron (yellow), bromide (dark green), oxygen (red), carbon (white) and hydrogen (light green).

The organic layer is built up from symmetry related [Dimim]+ counterions (0.5-x, 0.5-y, -z). This layer can be seen as [Dimim]+ zigzag chains extended along the *b*-axis, where the counterions are related by inversion centre symmetry. The adjacent chains are shifted $b/2$ respect to each other, following a *ABAB* sequence along the *a*-axis. The organic molecules are pillared along the *c*-axis and related through a *n*-glide plane, following a *ABAB* sequence. The shortest centroid-centroid distances between adjacent [Dimim]+ along the *b*-axis is 4.1679(1) Å. While the shortest interchain centroid-centroid distance within the *ab*-plane is 7.662(3) Å, distance which is notably shorter than the shortest inter-plane 8.6680(3) Å.

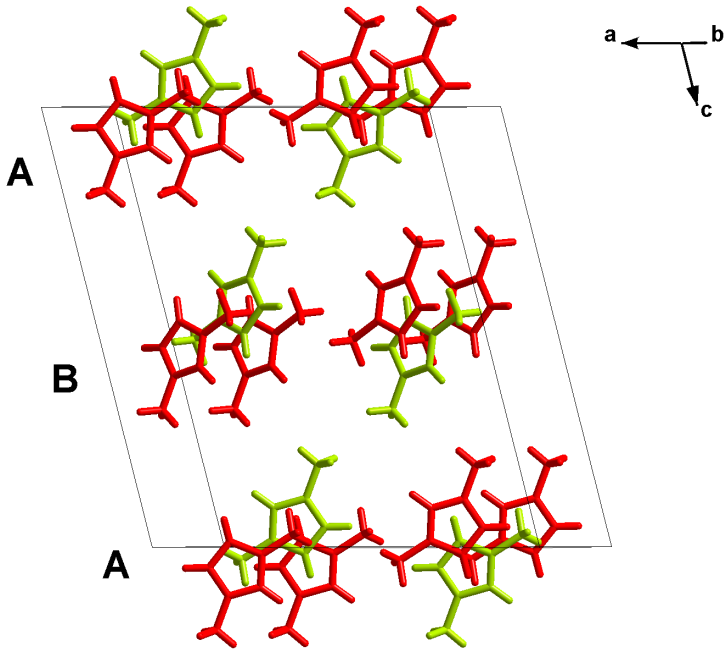

Figure 3.3: $[Dimim]^+$ configuration in the unit cell.

The inorganic layers are built up from dinuclear $[Fe_2OBr_6]^{2-}$ anions, formed by Fe^{3+} cation surrounded by three Br^- ions and one bridging oxo group. These units can be seen as two slightly distorted tetrahedron with an oxygen corner-shared. Each dinuclear unit is generated by the occurrence of a two-fold rotation axis along the *b*-axis, which lies on the oxygen atom [O(1)], giving rise to a bend angle between Fe-O-Fe of 166.5(2)°, value which is in good agreement with the previous reported for bent Fe-O-Fe units. [9] Moreover, due to the application of the two-fold rotation axis, the two $FeBr_3$ units are partially eclipsed with a torsion angle ranged from 47.94(3) to 67.88(3)°, and an angle between the two planes formed by the Br ions of each $FeBr_3$ unit is 11.966(10)°.

The dinuclear units are pillared in chains along the b-axis following a AA sequence. Each chain in the ab-plane is shifted $b/2$ respect to the adjacent one following a $ABAB$ sequence (see Fig. 3.5), while along the c-axis, these layers are related through a n-glide plane, following a $ABAB$ sequence (see Fig. 3.4). The intra-dinuclear Fe···Fe bond distance is 3.4993(8) Å from Fe(1)···Fe(1I) (I= -x, y, 0.5-z), while the shortest iron-iron distance within the ab-plane is 6.8524(7) Å from Fe(1)···Fe(1II) (II= 0.5-x, 0.5+y, 0.5-z), which corresponds to the distance between the shifted chains. Remarkably, this distance results to be shorter than the closest distance between irons within the chain, being 7.5979(8) Å from Fe(1)···Fe(1III) (III= x, -1+y, z). The shortest inter-plane distance between adjacent layers along the c-axis is 9.1567(9) Å from Fe(1)···Fe(1IV) (IV= x, 1-y, 0.5+z), being notably longer than the previously observed [8.57(1) Å] in the mono-nuclear Dimim[$FeBr_4$]. [16] The Br-Fe-Br bond angles in the inorganic unit range from 107 to 109°, which is in good agreement with the mono-nuclear Dimim[$FeBr_4$], while the mean distance Fe-Br is 2.3673(6) Å, which is shorter than the mono-nuclear distance. [16]

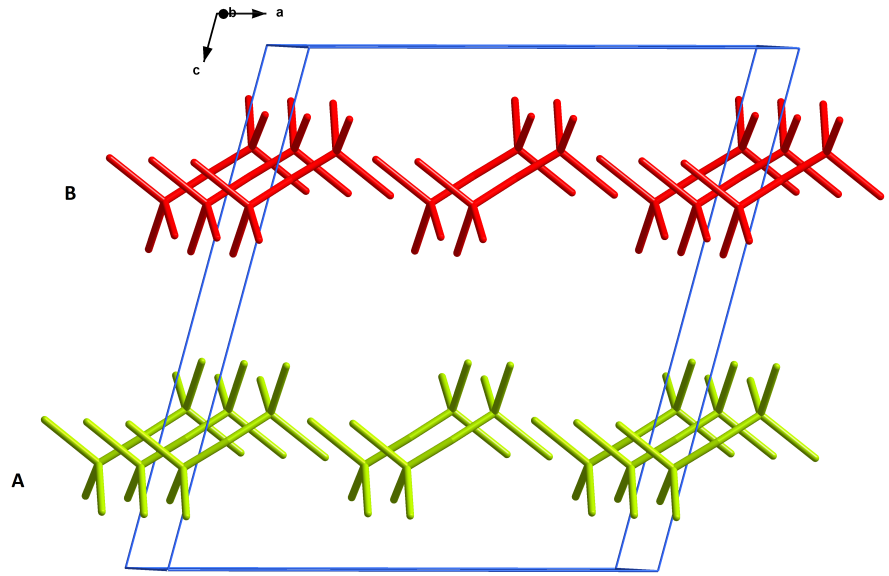

Figure 3.4: Inorganic chains along the b-axis. The solid blue line corresponds to the unit cell.

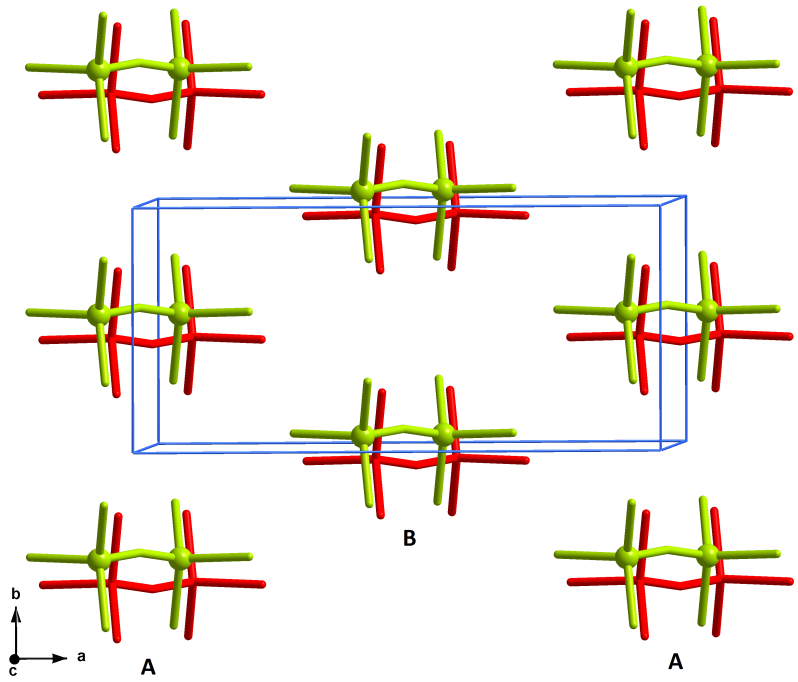

Figure 3.5: Disposition of the inorganic ions in the *ab*-plane. The solid blue line corresponds to the unit cell.

	Length / Å	Angle / º
N-methyl		
C6-N2	1.458(6)	
C6-N2-C2		126.3(3)
C6-N2-C4		125.6(3)
C1-N1	1.473(5)	
C1-N1-C2		125.8(3)
C1-N1-C5		125.6(4)
Ring		
C4-C5	1.347(4)	
C4-N2	1.383(6)	
C5-N1	1.386(5)	
C2-N1	1.318(5)	
C2-N2	1.339(5)	

Table 3.1: Interatomic distances in Dimim.

	Length / Å	Angle / º
[Dimim]···[Fe_2OBr_6] (potential $\pi - d$ interactions)		
Centroid···Br1	4.5212(4)	134.9(2)[a]
Centroid···Br3[i]	4.5638(4)	128.4(2)[a]
[Dimim]···[Dimim] (potential $\pi - \pi$ interactions)		
Centroid···Centroid[ii]	4.1672(1)	31.56(10)[b]

Table 3.2: Intermolecular distances in compound (**1**). [a]Angle between the plane formed by the aromatic ring and the Br.[b]Face-off angle (angle between the plane formed by the [Dimim] aromatic ring and the vector connecting both centroids). [Symmetry codes: (i) x, -y, -0.5+z, (ii) 0.5-x, -0.5-y, -z].

	Length / Å	Angle / º
Fe-Br		
Fe-Br1	2.3635(6)	
Fe-Br2	2.3663(7)	
Fe-Br3	2.3704(1)	
Fe-O-Fe		
Fe-O	1.7620(5)	
Fe···Fe	3.4993(8)	
Fe-O-Fe		166.5(2)
Br···Br		
Br1···Br2	3.8339(1)	
Br2···Br3	3.8223(1)	
Br3···Br1	3.8609(2)	
Br1-Fe-Br2		108.304(9)
Br2-Fe-Br3		107.595(2)
Br3-Fe-Br1		109.291(2)
Fe-O-Br		
Fe-O-Br1		110.2(5)
Fe-O-Br2		111.4(3)
Fe-O-Br3		110.1(3)

Table 3.3: Interatomic distances in $[Fe_2Br_6O]^{2-}$

	length / Å			Angle /º
D-H···A	*H···A*	*D-H*	*D···A*	*D-H···A*
C4-H3···Br2^{i}	2.95(5)	0.94(5)	3.77(3)	147(4)
C2-H1···Br2^{ii}	2.99(4)	0.94(4)	3.82(4)	148(3)
C5-H2···Br3^{iii}	2.95(5)	0.90(6)	3.71(4)	143(4)
C1-H9···Br3^{iii}	3.02(7)	0.99(7)	3.92(6)	152(5)
C6-H6···Br3^{ii}	3.06(6)	0.89(6)	3.83(5)	146(4)

Table 3.4: Hydrogen-bond geometry. *D* attends for donnor and *A*, for acceptor. Symmetry codes: (i) -x, 1-y ,-z, (ii) 0.5-x, 0.5-y, -z, (iii) 0.5-x, y-0.5,0.5-z.

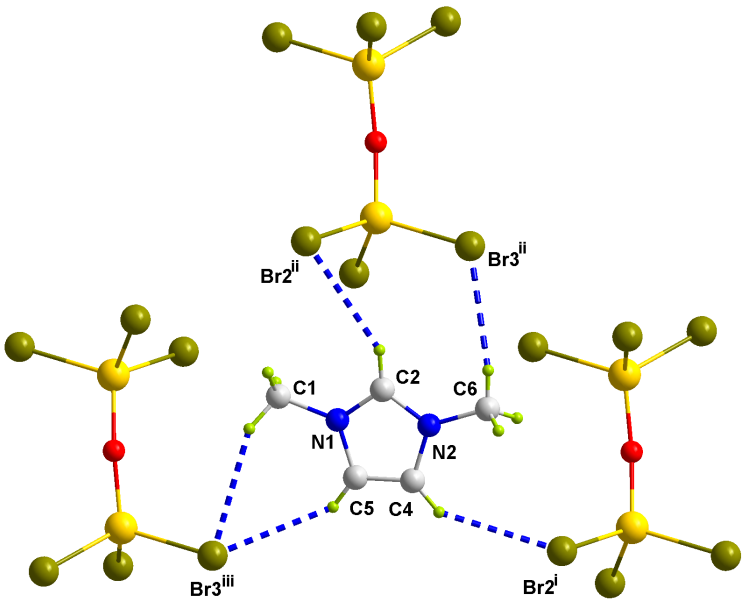

Figure 3.6: Hydrogen-bonding network in $Dimim_2[Fe_2OBr_6]$ (H-Br distances up to 3.1 Å are marked with blue dashed lines). Symmetry codes: (i) -x, 1-y ,-z, (ii) 0.5-x, 0.5-y, -z, (iii) 0.5-x, y-0.5,0.5-z.

According to the data presented in table 3.4, the main interactions are H-bond type, as we can see in Fig. 3.6, where the distances represented are shorter than the sum of the Van der Waals radii of hydrogen and bromide (1.2 and 1.85 Å, respectively). On the other hand, there could be $\pi - d$ interactions between the molecules, but they would be extremely weak, as the distance between them is considerably large (the maximum distance for these kind of bonds is usually around 4.3 Å). It is also possible the presence of $\pi - \pi$ bonds between adjacent $[Dimim]^+$ ions, as the distance between their centroids is shorter than in the previous case, but, although the planes formed by their rings are essentially parallel, they are not face to face but inverted respect to each other (n-glide plane). In consequence, we can conclude that the structure of compound (**1**) is sustained primarily by Van der Waals, hydrogen bonds and ionic interactions. These interactions are the weakest of their kind, which explains the low melting point and the existence of several phase transitions in a short range of temperatures (see sections 3.2 and 3.4).

3.2 Synchrotron Powder Diffraction

Powder diffraction patterns at different temperatures of compound (**1**) are presented in this section. The first and most obvious result is the existence of a solid-solid phase transition when cooling down from RT to 100 K and warming up again to RT, where it shows a different pattern from the first one. This difference between both patterns at 300 K is noteworthy, as one would expect to present the same phase at the same temperature. It is possible to distinguish clearly these distinct phases in Figs. 3.7 (initial RT and 100 K) and 3.8 (initial and final RT).

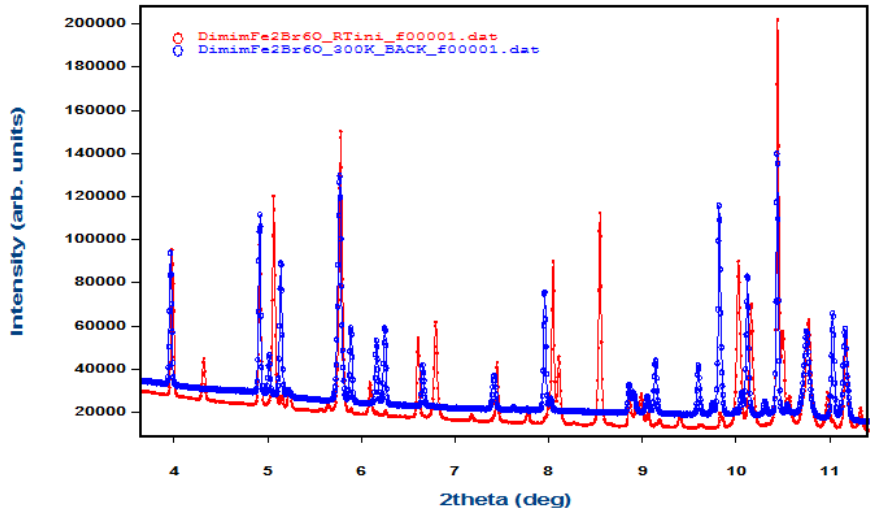

Figure 3.7: Synchrotron X-Ray diffraction patterns of compound (**1**) at 300 K (red points) and 100 K measured at ALBA synchrotron. A phase transition is clearly observed.

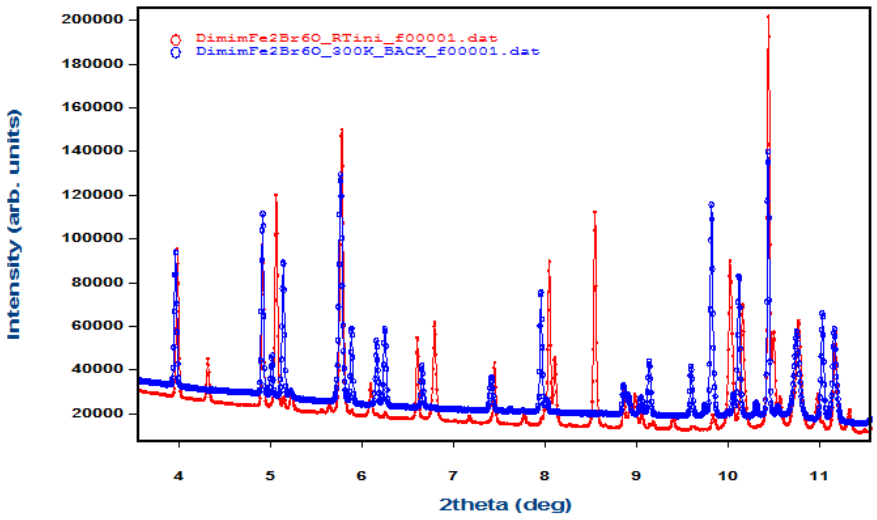

Figure 3.8: Synchrotron X-Ray diffraction patterns of compound (**1**) at the initial 300 K (red points) and final 300 K measured at ALBA synchrotron. A phase transition is clearly observed.

We attempted to refine the diffractograms corresponding to both initial and final RT and 100 K from the resolved single-crystal structure described in section 3.1 with no success. Likewise, a mixture of two phases, composed by the dinuclear and the mononuclear precursor structures did not adjust the pattern either, as can be seen in Fig. 3.9. This striking result can be due to different reasons. One explanation could be that the sample degrades as time passes outside the mother liquor in contact with air (the starting salts were highly hygroscopic) or due to the X-ray radiation damage. Another interpretation could be the presence of impurities different from the precursor monomers, being this last explanation the most unlikely, as most of the product resembled similar to the single-crystal from which the structure was determined. Furthermore, if these kind of crystals were present in the sample powder, even in a small percentage, all their corresponding reflections should appear in the diffractogram, which is not the case. We can see the absence of these peaks at 8.4º, for instance, corresponding to the planes (-4,0,2), (2,0,2), and (-3,1,3).

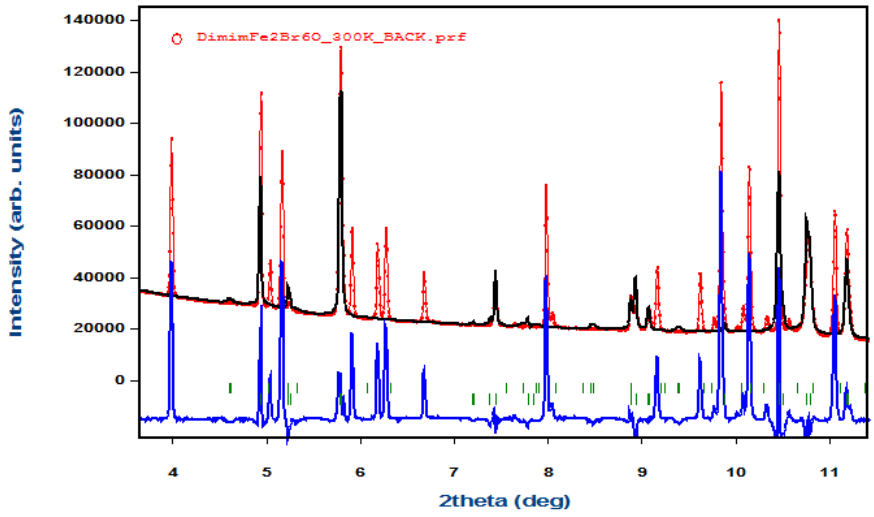

Figure 3.9: Synchrotron X-Ray diffraction pattern (red points) of compound (**1**) at RT measured at ALBA synchrotron. The refinement (solid black line) was performed from the mixture of two phases: the structure of (**1**) described in section 3.1 and the one of the precursor. The vertical green lines below the pattern correspond to the reflections of both phases, being the upper ones for the dinuclear and the lower ones for the mononuclear structure. The solid blue line corresponds to the difference between the pattern and the refinement.

3.3 IR and Raman spectra

The infrared and Raman spectra of complex (**1**) are shown in Fig. 3.10 and 3.11, respectively.

The infrared mode commonly used to characterize the oxo-bridge in iron(III) compounds is the antisymmetric stretch $\nu_{as}(Fe-O-Fe)$. This appears as a broad, strong band at 820-840 cm^{-1} and sometimes a shoulder is observed at 860 cm^{-1}. [23] These bands have been reported in other studies between 830 and 890 cm^{-1}, [11]. Moreover, broad bands at 648-680 cm^{-1} have been reported as well for the vibration mode $\nu(Fe-O)$. [24] All this is consistent with the IR spectrum of the dinuclear compound (**1**), which shows two strong, broad bands at 630-700 cm^{-1} and 840-900 cm^{-1} that are not observed in the case of the mononuclear precursor.

Regarding Raman spectroscopy, characteristic bands for the symmetric stretch $\nu_{sym}(Fe-O-Fe)$ have been reported in previous studies around 440-460 cm^{-1} and 362 cm^{-1}. [11] [25] [24] Therefore, the peaks that appear in Fig. 3.11 at 370 cm^{-1} and 416 cm^{-1} can be assigned to this vibration mode of the μ-oxo dinuclear iron(III) complexes, as they do not appear in Dimim[$FeBr_4$]. In this case, it is reasonable to assign two peaks to the same vibration mode on account of the nature of the compound (**1**), which seems to present two types of dimers (as already mentioned in section 3.2). On the other hand, the peak at 170 cm^{-1} seems to be the same one occurring at 153 cm^{-1} for the precursor but shifted possibly due to the packing variation.

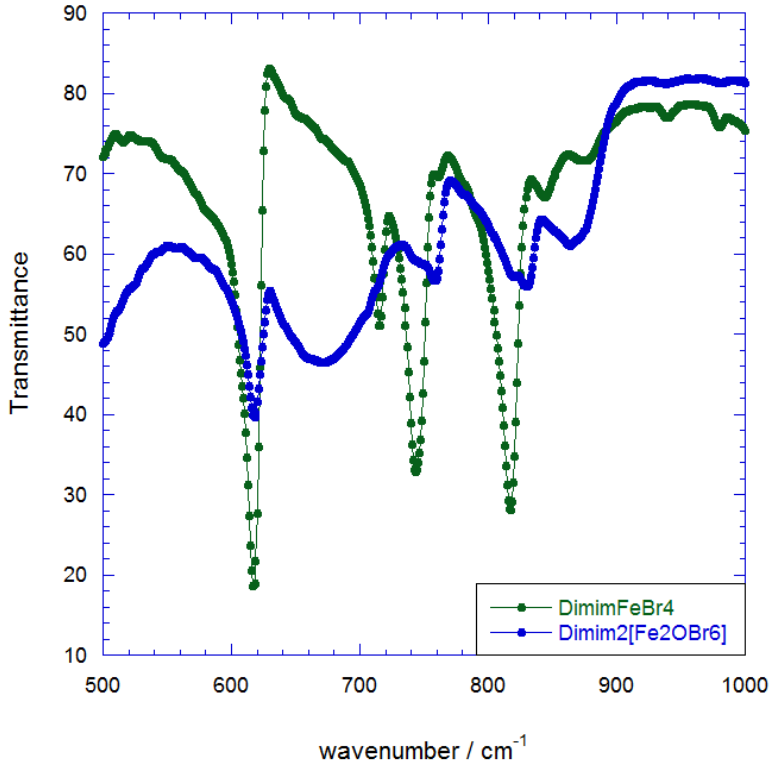

Figure 3.10: Infra-red spectrum of compound (**1**) (blue) and the mononuclear precursor (green).

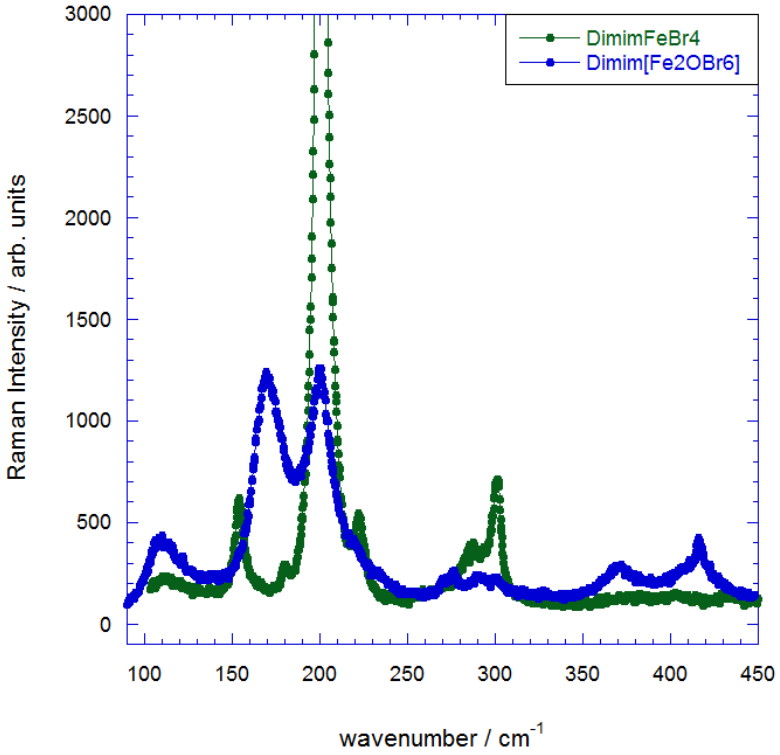

Figure 3.11: Raman spectrum for compound (**1**) (blue) and the mononuclear precursor (green).

3.4 Differential Scanning Calorimetry

In these section, the DSC measurements of compound (**1**) together with those of their two recrystallizations (compounds (**2**) and (**3**)) and their mononuclear precursor are shown in Figs. 3.12, 3.13 and 3.14, respectively.

The dinuclear compound (**1**) shows a solid-solid (s-s) phase transition around 73C upon heating from below the melting point (78C)[1], named phases I and II in Fig. 3.12. This s-s transition is observed also in the precursor around 90C and other MILs based on imidazolium ions. [17] [26] In the mononuclear complex, the aforementioned transition occurs together with the melting, at higher temperature than that of the dinuclear solid-liquid transition. This fact is consistent with the determination of the structure of (**1**), as the forces involved are much weaker than those in the precursor.

[1]The s-s transitions are distinguished from s-l transitions by their size. The latter require less energy than the former (no need to destroy all the bonds) and, therefore, less variance in the heat flow.

Compound (**3**) presents this phase transition too, although there is more temperature difference with the melting point. In Fig. 3.13b we can see the s-s phase transition at lower temperature than that of compound (**1**), around 65C, whereas the melting point is remarkably higher, around 107C. As regards for compound (**2**), the s-s transition is not observed, although it is not totally clear.

During the cooling cycle no phase transition is observed in compound (**1**) until it reaches a temperature around 40C, where a slight decrease in the heat flow is observed. This corresponds to an exothermic reaction and it can be due to the transition to a vitreous phase (named III in Fig. 3.12), although this is not utterly certain. This behavior is not observed in the rest of samples studied in this section, but all of them present different responses. In the case of the precursor, after solidifying at 80C, it suffers another s-s transition at 60^{o}C approx. and it remains stable after that until -73C. On the contrary, compound (**3**) only experiments one liquid-solid transition at 79C. Once again, the situation is not clear for compound (**2**): two peaks of the same magnitude appear together around 83C and 79C and a remarkably smaller one can be observed at 60C. This could be attributed to a solidification and two concatenate s-s transitions, but this cannot be determined without further research (X-ray diffraction).

To conclude, one more peak appears in compound (**1**) and compund (**2**) during the thermal stabilization at RT. In the first case, it corresponds to the beginning of the solidification of the sample, although the temperature should have been lowered in order to see the full transition[2]. It is noteworthy that this peak arises during the thermal stabilization at 25C and not before, during the cooling. As the difference in temperature between the melting point and the crystallization is remarkably elevated (almost 55C), the sample was left at 40C for 15 min. during the first complete DSC cycle to elucidate if the sample required a thermal stabilization to solidify, but no phase transition was observed.

[2]The area of the peaks from the heating and cooling cycles should be equal so that the absorbed and released energy is the same.

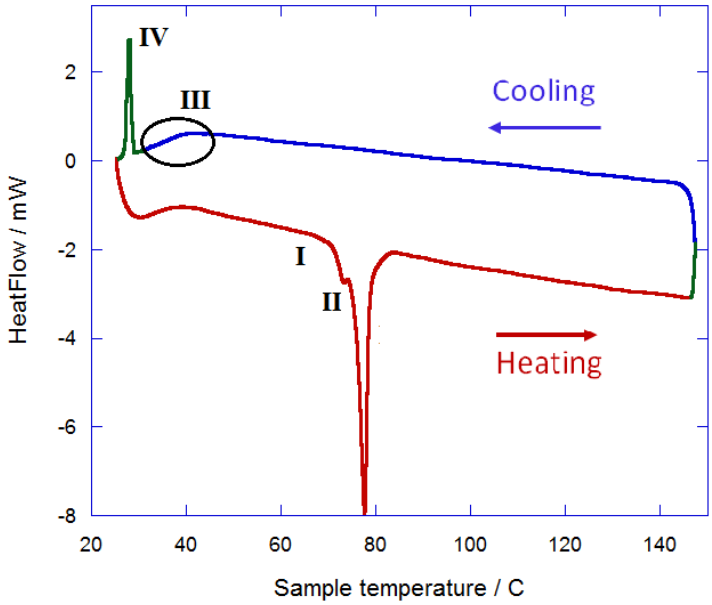

Figure 3.12: Second DSC of compound (**1**). The heating and cooling ramps were measured at 10 K/min, while the green solid lines correspond to the thermal stabilization steps.

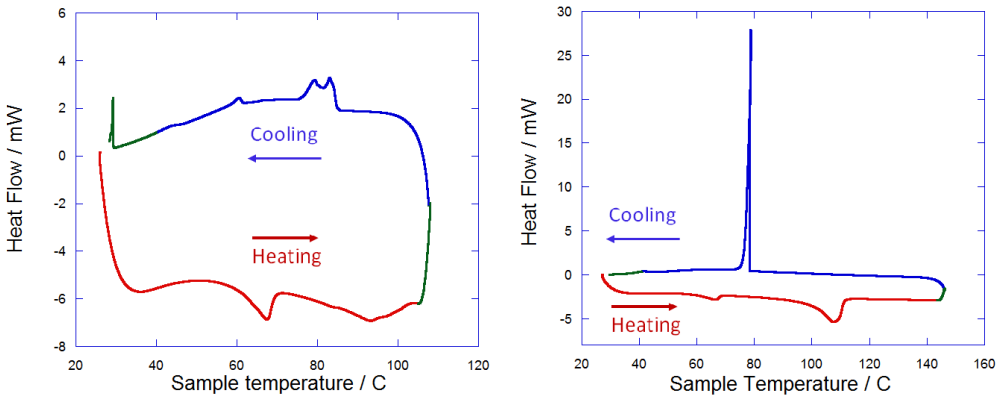

(a) (b)

Figure 3.13: Second DSC of both recrystallizations of compound (**1**) in 2-Propanol (a, compound (**2**)) and 1-Heptanol (b, compound (**3**)). The heating and cooling ramps were measured at 5 K/min, while the green solid lines correspond to the thermal stabilization steps.

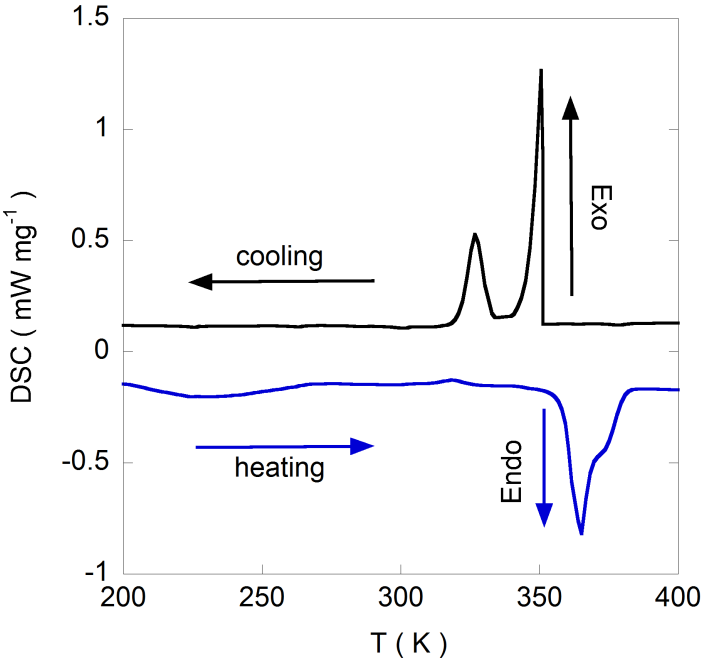

Figure 3.14: DSC of the mononuclear precursor Dimim[$FeBr_4$]. Figure extracted from Ref. [8].

3.5 Magnetic characterization

Solid-state, variable-temperature (2–300 K) magnetic susceptibility data (χ_m is the molar magnetic susceptibility per two Fe^{III} ions) in the form of both χ_m and $\chi_m T$ versus T plots under applied dc field of 1000 Oe are shown in Fig. 3.15. The data for compound (**1**) exhibit a behavior characteristic of antiferromagnetic species, where the magnetic values $\chi_m T$ drop sharply on lowering the temperature from a value of 8.72 cm^3 mol^{-1} K at 300 K to nearly zero at 2 K. As expected, the slope of this descent in $\chi_m T$ is much higher than in the monomer due to the remarkable stronger antiferromagnetic interactions between oxo-bridged irons. [16] The magnetic susceptibility, on the other hand, increases when the sample is cooled down until it reaches a sharp maximum around $T_N = 10$ K, where the system acquires long-range antiferromagnetic ordering.

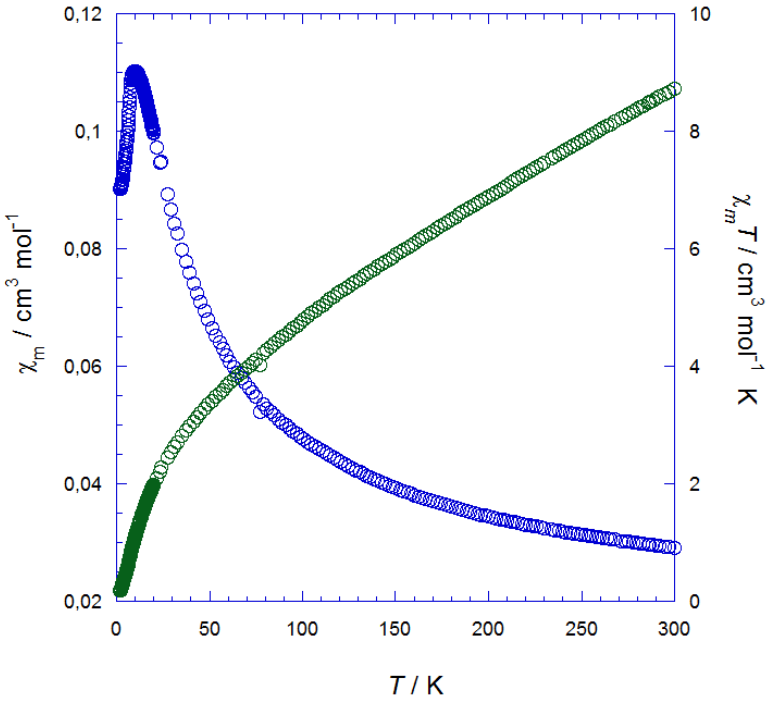

Figure 3.15: Temperature dependence of χ_m (blue) and $\chi_m T$ (green) measured under 1 kOe.

We attempted to fit the magnetic susceptibility data to the Van Vleck equation, derived from the spin exchange Hamiltonian for an isotropic dinuclear Fe compound (Eq. B.2). This model corresponds to high-spin dinuclear iron(III) compounds, employed succesfully in Ref. [12].

$$\chi = \frac{2Ng^2\mu_B^2}{kT}\frac{e^x + 5e^{3x} + 14e^{6x} + 30e^{10x} + 55e^{15x}}{1 + 3e^x + 5e^{3x} + 7e^{6x} + 9e^{10x} + 11e^{15x}}(1-p) + p\frac{35N\mu_B^2}{k(T-\theta)} \tag{3.1}$$

In the former expression, p represents the fraction of the paramagnetic impurity and $x = J/kT$, being J the coupling constant. Where N, k and μ_B are Avogadro's number, Boltzmann constant and Bohr magneton, respectively.

Nevertheless, this model only fits the data for low values of g (around 1.2), which is physically meaningless, and did not adjust at all when g was forced to be 2. This disagreement with the theoretical curve can be due to different motives: either a more complex model is needed to describe the magnetic structure (chains of dinuclear units, for instance) or there is a strong presence

of impurities. However, these impurities cannot be the mononuclear units, as the second term of Eq. 3.1 already accounts for this contribution.

Despite the failure in fitting the model, the value of $\chi_m T$ at RT for one iron atom (4.36 cm^3 K mol^{-1}) is consistent with the theoretical value ($(4/g^2)\chi T = 4.377$ cm^3 K mol^{-1} for a $S = 5/2$ atom, according to Ref. [27]) and coincides with previous studies of similar compounds (see Ref. [28]).

On the same way, the value for the effective magnetic moment μ_{eff} at 300 K ($5.917(1)\mu_B$) is in agreement with the theoretical value for one iron atom ($5.92\mu_B$), which is defined as:

$$\mu_{eff} = \sqrt{\frac{3k}{N\mu_B^2} \cdot \chi T} = \sqrt{8 \cdot \chi T} \tag{3.2}$$

Nevertheless, these values differ from those reported in the aforementioned work of Jui-Cheng Chang *et al.*. [12] This is due to the fact that these compounds show antiferromagnetic interactions even at RT, so that we cannot consider the magnetic atoms as two isolated iron centers anymore.

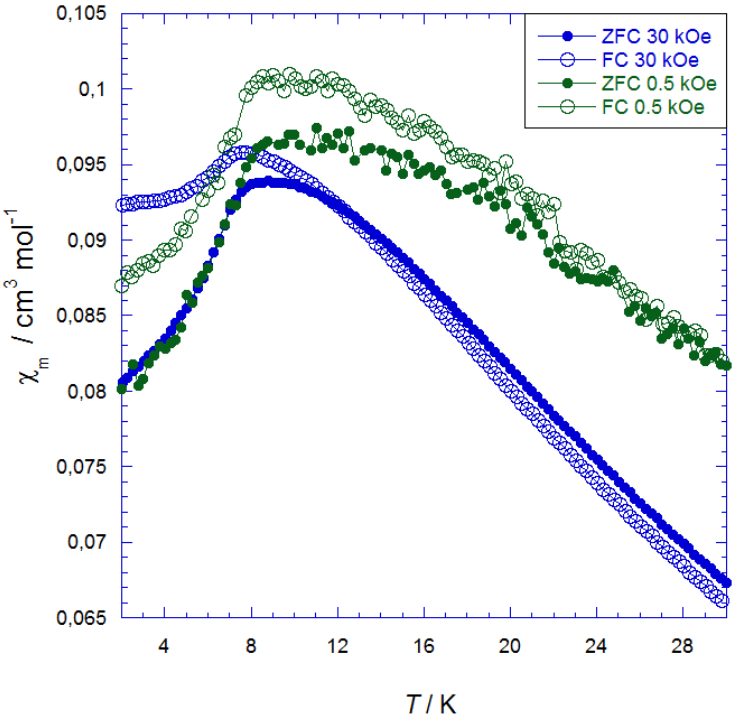

Figure 3.16: Low temperature ZFC-FC magnetic susceptibility for different magnetic fields.

A splitting in the molar susceptibility of the sample in the ZFC-FC[3] can be observed in Fig. 3.16. This irreversibility can occur due to the presence of ferromagnetic domains. Both curves show the same behavior: the molar susceptibility increases with decreasing temperature until it reaches a maximum value around 8.5 K and it smoothly decreases with temperature (indicating once more the antiferromagnetic nature of the material). The splitting is produced in this last stage, showing higher values of the susceptibility in the FC curve. As stated before, this phenomenon is produced because a fraction of the magnetic moments have been previously oriented by the magnetic field during the first heating ramp. In this scenario, the spins would be aligned antiferromagnetically not completely antiparallel to each other, but forming a small angle between them, inducing a extremely weak ferromagnetic component.

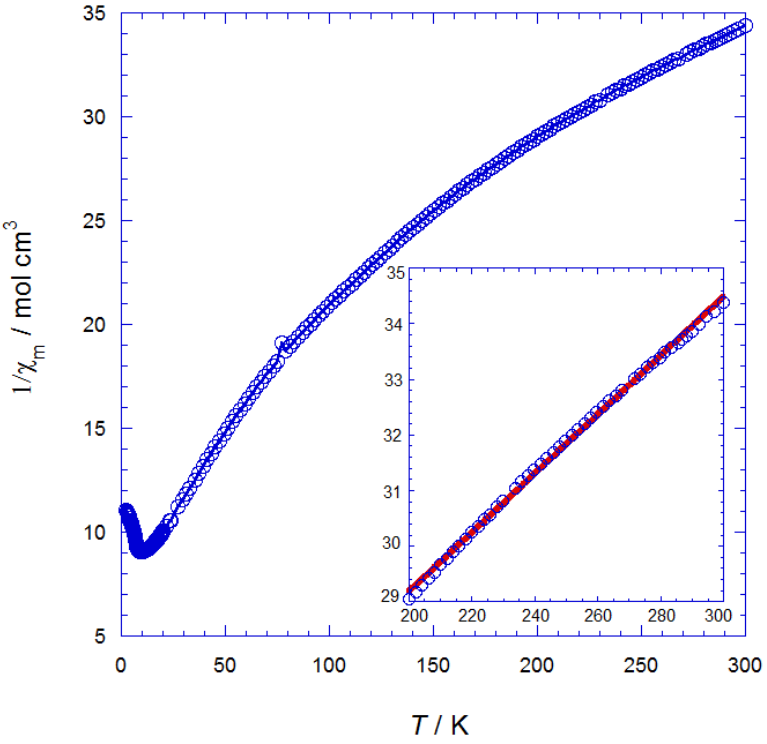

Figure 3.17: Temperature dependence of $1/\chi_m$ measured under 1 kOe (blue circles). The inset shows the fit to the Curie-Weiss law in the paramagnetic region (200-300 K).

[3]ZFC-FC stands for Zero Field Cool-Field Cool. This means that the sample was cooled under no external magnetic field and then the susceptibility measurements were taken while heating and cooling again under applied field.

The behavior of a ferro- or antiferro-magnet in the paramagnetic region is described by the well-known Curie-Weiss law, which is the Curie law displaced by an amount θ_p (which has positive values for the case of ferromagnetism and negative values for antiferromagnetism), and is given by the expression:

$$\chi_m = \frac{C}{T - \theta_p} = \frac{N\mu_0\mu_{eff}^2}{3k(T - \theta_p)} \tag{3.3}$$

Being C and θ_p the Curie and Weiss constants, respectively.

According to Eq. 3.3, the inverse of the susceptibility should present a linear behavior respect to the temperature. This is not the case, as can be observed in Fig. 3.17, meaning that the behavior cannot be described as paramagnetic. This feature of the compound evidences once more the strength of the antiferromagnetic interactions between irons. Likewise, the aforementioned weak ferromagnetism can contribute to this deviation from the Curie-Weiss law.

Nonetheless, the susceptibility curve was fitted to this law in the higher range of temperatures where it should have a more paramagnetic behavior. This fit is shown on the inset of Fig. 3.17, which gives a value for the $\mu_{eff} = 8.69(3)$ μ_B per two iron atoms and a θ_p value of -351(4) K, which is extremely high compared to the mononuclear precursor (-14.9 K). Despite the roughness of this procedure to estimate the Weiss constant and the effective magnetic moment, it results enough to verify that the former has a negative value and is much greater than that of the monomer, as was expected due to the stronger interactions between irons inside the inorganic molecule.

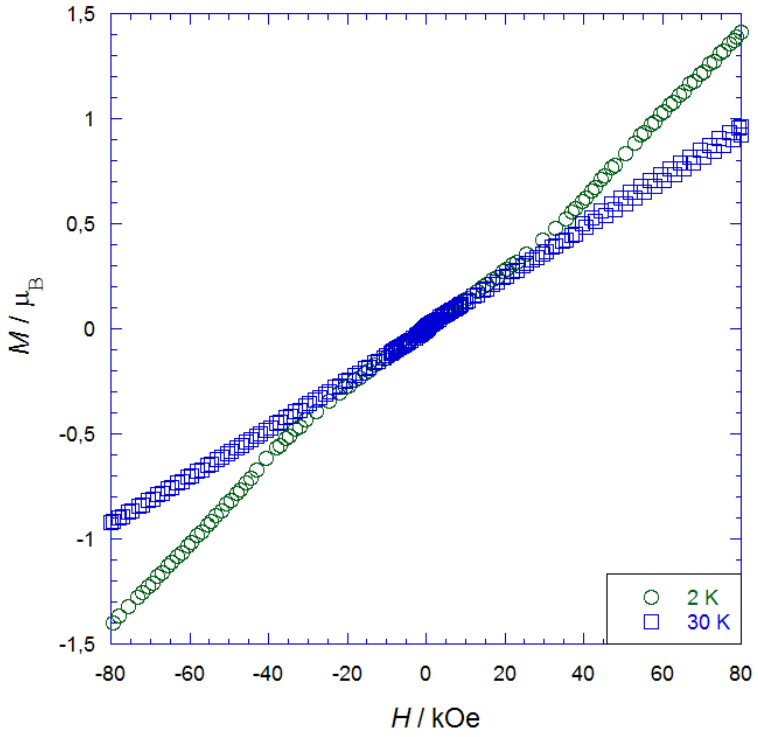

Figure 3.18: Magnetization as a function of the applied magnetic field at two different temperatures.

Regarding the magnetization measurements, shown in Fig. 3.18, M at 30 K shows a linear dependency in the whole applied field range confirming the paramagnetic behavior at this temperature. It is also noteworthy the presence of an inflection point around 35 kOe. This is also reported in the mononuclear precursor under the same temperature and field conditions (see Ref. [16]) and could indicate the existence of a metamagnetic transition, probably meaning an increase in the angle between spins. On the other hand, the magnetization increases smoothly with the applied field showing no evidences of saturating, which is consistent with the strong magnetic structure, as the highest field you apply is not strong enough to turn over the spins. The hysteresis only appears at low fields and could only be observed zooming the range between 100 and 200 Oe of the 2 K curve, which highlights the weakness of the ferromagnetic component.

CHAPTER 4

Conclusions

A new 3D magnetic correlated ionic liquid based on imidazolium cation and tetrabromoferrate ions, namely $Dimim_2[Fe_2OBr_6]$, was synthesized and structurally characterized during this project. The main conclusions extracted from the results obtained will be summarized below.

Firstly, compound (**1**) presents long-range antiferromagnetic ordering below 10 K, slightly higher than the ordering temperature of its precursor (8 K). This result is compatible with the structure of the compound, as the antiferromagnetic interactions were expected to be extremely greater than those in the mononuclear complex. On the other hand, the magnetic susceptibility data did not fit the theoretical model for high spin Fe(III) dinuclear compounds. Further study is needed to disentangle the causes of this disagreement with the theoretical expression as well as the discrepancy between the synchrotron diffraction measurements and the structure solved by single crystal X-ray diffraction. Plausible explanations could be the presence of impurities, the existence of two kinds of dimers, the deterioration of the sample (because of being irradiated or extracted from the mother-liquor) or the need for a more complex model to adjust the χ_m curves.

Regarding the nuclear structure, it is worthy to mention that the forces sustaining it are weaker than in the precursor, as the lengths between molecules are larger. This is corroborated by the DSC measurements, which show a lower melting point, as less energy (heat flow) is needed to break the bonds within the sample.

Although we know the nature of the magnetic interactions, we are in the dark about the compound's magnetic structure. The determination of this arrangement will be accomplished by future neutron diffraction measure-

ments at Institut Laue-Langevin.

To conclude, the other products obtained were characterized by FTIR and some of them by Raman spectroscopy, magnetic measurements and DSC. Nevertheless, it is not possible to secure the presence of dinuclear units only by these techniques. Hence, X-ray diffraction is needed to determine their structure on the same way than it was done for compound (**1**).

APPENDIX A

Principles of X-Ray diffraction and the Rietveld method

X-Ray diffraction provides information about the spatial ordering of the atoms in a crystal on the following way. When the radiation incises in a material, it excites the atoms' electrons and is scattered on such a way that interferences are produced between the scattered beams, depending on the incidence angle (θ) and the distance between the crystallographic planes d. The condition for the beams to be in phase is called the Bragg's law and it is given by the expression:

$$n\lambda = 2d_{hkl}sin\theta_{hkl} \tag{A.1}$$

Where n is a natural number, λ is the wavelength of the incident radiation and hkl refer to the Miller indexes.

This geometrical approach can also be described using the Drude-Lorentz model, which assumes the atomic nuclei fixed in the crystal net and the electrons submitted to a elastic force which makes them oscillate around the positive ions, while the free electrons are the responsible for the electrical conductivity[1]. Therefore, the bonded electrons which are describing a harmonic oscillator movement acquire the same frequency than that of the incident beam, emitting it in turn (because they are accelerated) with certain phase difference between one nucleus and the next one (the electrons are excited as light travels inside the material). This phase difference is what originates the interferences that create the diffraction pattern to analyze.

Each peak of this difractogram corresponds to a crystallographic plane, which permits to know which peaks appear and which ones do not to determine the crystal structure. The process to assign its corresponding plane to

[1]These free electrons are not relevant for the X-ray analysis

each peak is called indexing, and it is usually the most complex step when studying the structure of a crystalline sample.

The last method to gather structural information is the study of the peaks' intensity ratios. These intensities are given by the expression:

$$I_{hkl} = K \cdot m_{hkl} \cdot L_\theta \cdot P_\theta \cdot A_\theta \cdot T_{hkl} \cdot E_{hkl} |F^2_{hkl}| \tag{A.2}$$

Where K is just a scalar constant, m_{hkl} is the multiplicity[2], F_{hkl} is the structure factor, which gives information about the unit cell's diffracting power. The rest of variables are related to the extinction, absorption, preferential orientations, etc. As all these parameters are intrinsic within the material and what we are interested in is the ratio between intensities, not the absolute intensities themselves[3]. Therefore, what really provides information is the structure factor, as it is related to the intensity ratios on the form:

$$\frac{I_{hkl}}{I_{h'k'l'}} = \frac{m_{hkl}|F^2_{hkl}|}{m_{h'k'l'}|F^2_{h'k'l'}|} \tag{A.3}$$

The structure factor is given, in turn, by the expression:

$$\begin{aligned} F_{hkl} = \sum_{j=1}^{n} f_j [cos 2\pi (hx_j + ky_j + lz_j) \\ + i \cdot sin 2\pi (hx_j + ky_j + lz_j))] \end{aligned} \tag{A.4}$$

Where f_j is the atomic diffraction factor of each type of atom j and x_j, y_j y z_j are the coordinates of each atom j in the unit cell (the motive of the crystal).

All the procedure described here to determine the crystal structure of a compound is known as the Rietveld method, which is normally applied with the help of specialized softwares.

[2]The multiplicity corresponds to the number of possible combinations of hkl. In powder X-ray diffraction, the plane 331 of a cubic crystal, for instance, contributes to the intensity of the same peak than the plane 313, unlike in single-crystal X-ray diffraction.

[3]It has no sense to speak about the absolute peak's intensity because it is necessary then to know all the details about the functioning of the diffractometer and calibrate it, which is not trivial.

APPENDIX B

Isotropic interactions in dinuclear compounds

In order to fit the magnetic susceptibility of the compound **1** to a theoretical model, we must consider the interaction between two magnetic centers within the molecule. The Hamiltonian describing this situation is the so-called Heisenberg-Dirac-Van Vleck (HDVV) Hamiltonian. Even though the interaction between the two atoms is purely electrostatic, it is often described by the coupling of the two local spin operators S_A and S_B. The phenomenological Hamiltonian accounting for this may be written as

$$\vec{H} = -J\vec{S_A}\vec{S_B} \tag{B.1}$$

Where J is the isotropic exchange integral between the A and B atoms and is negative in the case of antiferromagnetic exchange.

This expression is valid for any pair of interacting magnetic centers with local spins S_A and S_B, provided that the local states have no first-order angular momentum. In this case we consider the two magnetic centers are identical, with $S_A = S_B = 5/2$, and symmetry related within the dinuclear unit. the total spin Hamiltonian taking into account the Zeeman perturbation is then: [27, Ch. 6]

$$\vec{H} = -J\vec{S_A}\vec{S_B} + \beta(\vec{S_A}\vec{g_A} + \vec{S_B}\vec{g_B})H \tag{B.2}$$

where $\vec{g_A}$ and $\vec{g_B}$ are the local g-tensors, which, in our hypothesis, are equal.

From this Hamiltonian, it is possible to derive the expression for the magnetic susceptibility applying the Van-Vleck Formula: [27, Ch. 1]

$$\chi = \frac{N\sum_n E_n^{(1)2} exp(-E_n^{(0)}/kT)}{kT\sum_n exp(-E_n^{(0)}/kT)} \tag{B.3}$$

Where $E_n^{(0)}$ is the energy of level n in zero field. $E_n^{(1)}$ and $E_n^{(2)}$ are called first- and second-order Zeemann coefficients, respectively.

For high-spin iron(III), where $S_A = S_B = 5/2$, a set of spin-states, $S = 5, 4, 3, 2, 1, 0$ exist with energies $-15J$, $-10J$, $-6J$, $-3J$ $-J$ and 0, respectively. The energy level diagram is shown in Fig. B.1.

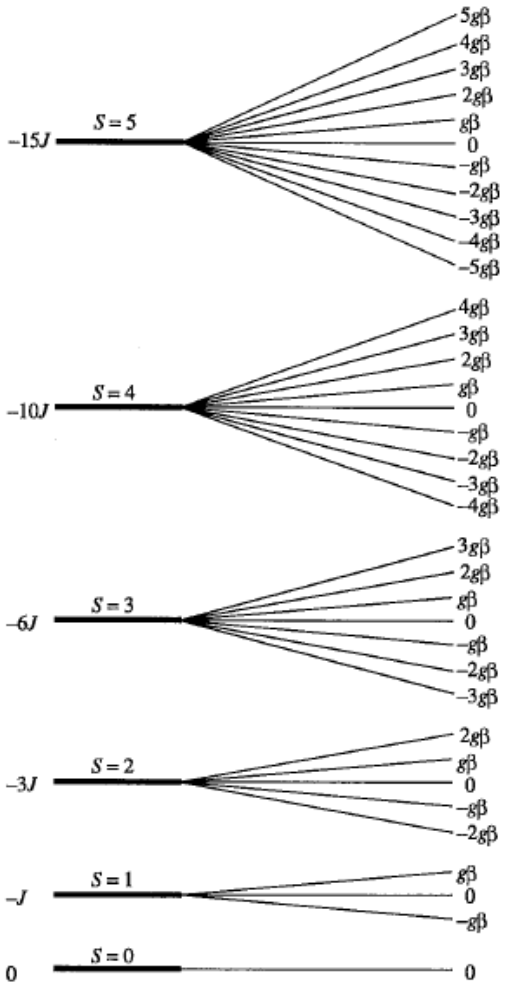

Figure B.1: Energy level diagram for a pair of interacting Fe^{3+}.

Thus, according to Eq. B.3, the final expression χ is:

$$\chi = \frac{2Ng^2\beta^2}{kT} \frac{e^x + 5e^{3x} + 14e^{6x} + 30e^{10x} + 55e^{15x}}{1 + 3e^x + 5e^{3x} + 7e^{6x} + 9e^{10x} + 11e^{15x}} \tag{B.4}$$

Where $x = J/kT$

APPENDIX C

Project proposals

The project proposals sent to Institut Laue-Langevin and Diamond Light-Source for neutron diffraction and XANES measurements, respectively, can be found attached in this section.

Summary of Proposal 14775

Related Proposal:	Resubmission of 10116
Requested Access Route:	Standard
Principal Investigator:	**Dr Jesus Chaboy, Instituto de Ciencia de Materiales de Aragón (ICMA)**
Alternate Contact(s):	Dr. Imanol de Pedro, University of Cantabria
Co-Investigator(s):	Ms Palmerina gonzalez, University of Cantabria Dr Sofia Diaz-Moreno, Diamond Light Source Dr Oscar Fabelo, Institut Laue-Langevin Professor Jesus Rodriguez Fernandez, University of Cantabria Dr Garikoitz Beobide, Universidad del Pais Vasco
Title:	**[Fe2X7] (X = Cl and Br) Ionic Complexes as Building Blocks for Room Temperature Magnetic Ionic Liquids with large magnetic response**
Primary Beamline:	I20-1
Shifts Requested:	9 **RCaH requested:** No
Industry Involved:	No **Industry Group Links:** No
Science Area(s):	Materials, Physics, Chemistry

Abstract: Magnetic Ionic Liquids (MILs) are a new class of smart materials which allow physicochemical properties to be controlled by external magnetic fields. In the search of developing new MILs with enhanced magnetic response at room temperature, we have synthetized a new family of MILs based on imidazolium cation and [Fe2X7]- anion, which constitutes a fundamental step for improving their technological applications .
High resolution XANES will allow the determination of the FeX7- dimers, and rule out the presence of other iron species. In addition the comparative study between the solid and the liquid-state speciation could reveal possible differences induced by crystallization. Moreover, new tailored dicationic MILs, like Emin[FeCl4]1-x[FeBr4]x (0 ≤ x ≥ 1), will be characterized as the different Fe-Cl and Fe-Br coordination can be easily disentangled.

Detailed Information:

Question	Answer
Please confirm you have checked the I20 website for the current status and conditions	Yes
Have you discussed your proposal with a member of the I20 staff?	yes
Have you any objections to this proposal being appraised for technical feasibility by the beamline staff?	No
What type of experiment are you planning to perform? Note: If both types of experiments are chosen then please respond to all the XAS and XES specific questions	X-ray Absorption Spectroscopy, XAS (transmission and/or fluorescence detection)
Which monochromator crystal cut do you need for your experiment? Currently only Si(111) is available. Please refer to the I20 webpage for information about energy ranges covered by the crystals.	Si(111)
For XAS experiments, which element and absorption edge are you planning to study?, if more than one, please indicate all of them	Fe K-edge
For XAS experiments, which detectors do you require?	Germanium 64 elements detector
For XES experiments, which element and absorption edge are you planning to study? Only one per experimental visit is allowed. If more than one element is required, several visits should be requested. Contact	Fe K-edge

Question	Answer
beamline staff to discuss your requirements.	
For XES experiments, what type of measurements do you wish to make?	High resolution XANES
For XES experiments, specify the emission line and energy that you are planning to measure in your experiment? (Example: Fe Kα1 6403.84eV , Cu Kβ 8905.29 eV, etc...).	Fe K-edge 6403.8 eV
For XES experiments, which crystal analyzer will you use for your experiment? Only one per experimental visit is allowed. If more than one crystal analyzer is required, several visits should be requested.	one
Which detectors do you require?	Silicon single element
Select one option, is your sample...	solid, Liquid
List all the samples you plan to use indicating the chemical formulae and chemical components	Emim[FeCl4]1-x[FeBr4]x ($0 \leq x \leq 1$)
What is the major component of each sample?	carbon and halure
What is the density of each sample (g/l)?	1.24 g/l
List the element and its concentration or total amount of the absorber in your samples. Indicate if the concentration is Molarity, Molality, Mole fraction, Stoichiometric atomic fraction or thin film	carbon iron hidrogen notrogen and halure
If your sample is air/moisture sensitive or need special handling, please specify the requirements.	Not applicable
For XAS which sample environment would you need for your experiment.	LN2 cryostream, Room Temperature
For XES which sample environment would you need for your experiment?	LN2 cryostream, Room Temperature
If bringing your own sample environment, please be specific in the description and contact the beamline staff to ensure the compatibility of the equipment and the need of support and integration to the beamline control system	Not applicable
Please indicate the operational temperature (units) of the measurements or the range of temperatures (units) required	Not applicable
If the experiment requires special synchronization of signals please specify and contact the beamline staff.	Not applicable
If you need to use gases in your experiment, please list them all.	Not applicable
Do you need cooling water for your experiment?	No
Do you plan to use I20 sample cells?	Yes
If not using I20 sample cells, please describe other specific environments you are planning to use at the beamline. Please contact the beamline staff if bringing your own	Not applicable
If you do require use of the spectroscopy village laboratories, select which ones.	Not applicable
If other Diamond laboratories are required, please specify	Not applicable
Select the equipment required from the instrumentation lab.	Not applicable
Select the equipment required from the chemistry lab.	Not applicable
Select the equipment required from the physics lab.	Not applicable
If the equipment that you need for your experiment is	Not applicable

Question	Answer
not listed, please specify your needs and we will try to find if it is available at Diamond.	

Samples:

Name	CAS No	Type	
1 Ethyl ,3 methylimidazolium tetrabromideferrate, EmimFeBr4 (Copy)	null	**ChemicalSubstance:**	liquid/solution
1 Ethyl ,3 methylimidazolium (p-Oxo)bis[trichalureferrate(III), EmimFe2Cl7 (Copy)	null	**ChemicalSubstance:**	liquid/solution
1 Ethyl ,3 methylimidazolium tetrabromideferrate, EmimFe2Br7 (Copy)	null	**ChemicalSubstance:**	liquid/solution
1 Ethyl ,3 methylimidazolium tetraclhorideferrate, EmimFeCl4 (Copy)	null	**ChemicalSubstance:**	liquid/solution

Experimental Method:	Method
Sample Preparation:	Diamond prep-lab required: Not required
Beamline Experiment and Environment:	Description of experimental set-up and procedures: cryostate
Experimental Method:	Method
Sample Preparation:	Diamond prep-lab required: Not required
Beamline Experiment and Environment:	Description of experimental set-up and procedures: cryostate

[Fe_2X_7] (X = Cl and Br) Ionic Complexes as Building Blocks for Room Temperature Magnetic Ionic Liquids with large magnetic response

Aims of the experiment and scientific background

The study of Magnetic Ionic Liquids (MILs) has been a new and emergent field since 2005. These materials allow physicochemical properties (viscosity, melting point, chemical stability, high ion conductivity, etc.) to be controlled by external magnetic fields[1] and can be used in the liquid state to formulate nanoparticle-free magnetic emulsions and microemulsions[2]. Therefore, during these last few years, the synthesis, study and application of these smart materials has increased exponentially[3], being also necessary to provide a complete picture of their crystal structure and main magnetic interactions in play.

Despite it was generally assumed that magnetic interactions were negligible in MILs, so they were not expected to exhibit 3D ordering[4], we have found that it is possible to synthetize MILs with three-dimensional ordering, which opens up new fields of understanding and improving the magnetic couplings within MILs[5]. The MIL resulting from mixing equimolecular amounts of FeX_3, where X=Cl or Br, and the halogen salt of 1ethyl-3 metylimidazolium (EmimX) displays a paramagnetic behaviour over most of the temperature range studied, with effective paramagnetic moments and paramagnetic Curie temperatures both anticipating an overall antiferromagnetic behaviour, and long-range magnetic ordering is detected at low temperatures[6]. Single crystals and power neutron diffraction experiments of the condensed phase shows that the main species in the solid state corresponds to Emim[FeX_4] (X=Cl and Br), showing Fe-Fe distances larger than 6Å[5]. No structural determination in the liquid phase has been attempt.

In the search of developing new MILs with enhanced magnetic response at room temperature, we have synthetized a new family of MILs by varying the molar ratio of the two reactants in such a way that the concentration of iron centres is doubled. These MILs show a much larger effective magnetic moment (μ_{eff} = 8.35 and 7.90 μ_B for Cl and Br, respectively), suggesting the formation of iron dimmers species, EminFe_2X_7 (X = Cl and Br). It has also been observed that these materials experience a solid-solid transition below ambient temperature. The determination of the type of molecular self-assembly of the iron species in the liquid state and the crystal framework of these MILs is a fundamental step towards the understanding of the origin of the enhanced magnetic properties. This will allow us to tailor made new materials, constituting a fundamental step for the technological applications of MILs.

We propose here to determine the local structure around the metallic centre by using X-Ray absorption Spectroscopy (XAS) at the Fe K-edge in MILs based on FeX_4 and Fe_2X_7 (X = Cl and Br) metal complexes, both in solid and liquid state. Although the presence of dimmers is very difficult to identify by EXAFS due to the large coordination distances, theoretical *ab-initio* calculations (see Fig. 1) indicate that by analyzing the XANES part of the spectrum it should be possible to determine the existence of $Fe_2X_7^-$ dimers, and to rule out the presence of FeX_4^- ions. The subtle differences expected show the need for collecting the XANES data with high resolution, aiming to enhance those differences. This can be accomplished by using the emission spectrometer available at the scanning branch of I20. For completion, we are planning to perform additional measurements of the solid compounds at LN_2 temperature, as we would like to determine if the solid-solid transition has any effect in the local environment around the iron centre.

In addition, we plan to extend our structural study to the characterization of a new family of dianionic magnetic ionic liquids, of the type Emim$[FeCl_4]_{1-x}[FeBr_4]_x$ ($0 \leq x \leq 1$). The theoretical simulations presented in Figure 2 show how the different Fe-Cl and Fe-Br coordination can be easily disentangled. This opens up a huge number of possibilities for the design of new tailored MILs for magnetic, spectroscopic, or catalytic properties.

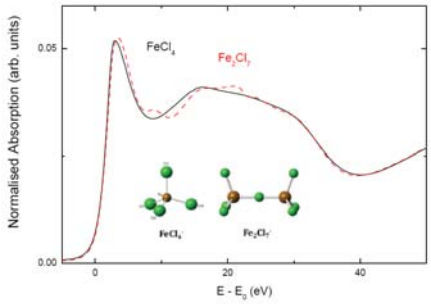

Figure 1. Comparison of the Fe K-edge XANES theoretical spectra computed for both $FeCl_4$ and Fe_2Cl_7 clusters

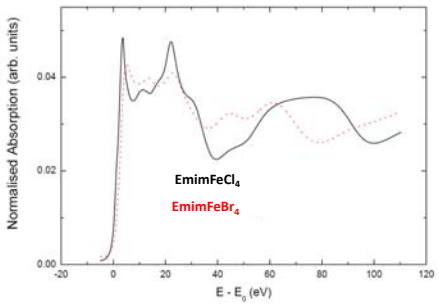

Figure 2. Comparison of the theoretical Fe K-edge XANES computed for $EminFeCl_4$ and for the same structure by replacing Cl by Br at the same structural positions.

Experimental method

We propose to perform a high resolution XANES study at the Fe K-edge on MILs based on $[FeX_4]^-$ and $[FeX_7]^-$ (X = Cl and Br) in both liquid and solid phases. The X-Ray Emission Spectrometer available in I20, equipped with three Ge(440) crystal analyzers will be used to perform the experiment by measuring the K_α emission line (6403.8 eV).

We estimate that nine shifts are necessary to complete the experimental programme described above. This will allow enough time to set-up the emission spectrometer and measure five samples in liquid and in solid state. Nine shifts will also be enough to setup the liquid nitrogen cryostat to carry out the low temperature (solid phase) measurements.

Results expected

The analysis of the XAS spectra recorded at the Fe K-edge will allow us:

i) to determine the structure in liquid phase of the species present in the MILs described. The high resolution measurements will allow us to confirm the existence of $[FeX_7]^-$ dimmers in the newly designed MILs.

ii) the comparative study between the solid and the liquid-state speciation by XANES will reveal any structural differences around the metal centre induced by crystallization.

iii) to characterize new diationic MILs (see Figure 2), like Emim$[FeCl_4]_{1-x}[FeBr_4]_x$ ($0 \leq x \leq 1$), for creating tailored room temperature ionic liquids to meet specific requirements.

These findings will open a promising route for the development of MILs with a primary focus in Materials Science; supported by the growing interest of chemists, physicists, and materials scientists in these materials.

References

[1] T. Torimoto, et al., *Adv. Mater.* **2010**, *22*, 1196.
[2] R. Dobbelin, et al., *Polym. Chem*. **2011**, *2*, 1275.
[3] T. Peppel, et al., *Angew. Chem. Int. Ed.* **2010**, *49*, 7116; A. Piecha, et al., *J. Mater. Chem*. **2012**, *22*, 333; M. Okuhata, et al.,*Chem. Commun*. **2013**, *49*, 7662.
[4] B. Mallick, et al., *Angew. Chem. Int. Ed.* **2008**, *47*, 7635.
[5] I. de Pedro et al., *J.Phys.: Condens. Matter* **2010**, *22*; *ibid. J. Magn. Magn. Mater.* **2011**, *323*, 1254. *ibid. Chem. A Eur. J.* **2014**, *20*, 72.
[6] A. García-Saiz, et al., *J. Phys. Chem. B* **2013**, *117*, 3198.

ILL RESEARCH PROPOSAL

Printed: 19/02/2016

Title: **Magneto-structural correlations onnew bimetallic-anionic paramagnetic ionic liquids with 3D magnetic ordering in its solid state.**	**5-31-2460**

Proposer (to whom correspondence will be addressed)

Name and first name	Address	Phone	Email
Manuel DE PEDRO DEL VALLE	**CITIMAC, UNIV SANTANDER** FACULTAD DE CIENCIAS UNIV CANTABRIA E-39005 SANTANDER SPAIN	34-942-201512 New neutron user: **No** New ILL user: **No** Local contact contacted: **Yes**	depedrovm@unican.es

Co-proposers

Name and first name	Laboratory	Country
FERNANDEZ DIAZ Maria Teresa	**ILL, GRENOBLE**	INSTITUT LAUE-LANGEVIN
FABELO ROSA Oscar Ramon	**ILL, GRENOBLE**	INSTITUT LAUE-LANGEVIN
GONZALEZ IZQUIERDO Palmerina	**ILL, GRENOBLE**	INSTITUT LAUE-LANGEVIN
RODRIGUEZ FERNANDEZ Jesus	**UNIV DE CANTABRIA, SANTANDER**	SPAIN
BEOBIDE Garikoitz	**FAC SCIENCE & TECH., UPV / EHU, LEIOA**	SPAIN

Local contact(s): **FERNANDEZ DIAZ Maria Teresa, FABELO ROSA Oscar Ramon**

Suggested keyword number: **5-31**

This proposal is:

- [x] A new proposal
- [ ] A continuation proposal
- [ ] A resubmission

Main research area: **Materials**

Submitted to other facilities: **No**

Societal indicators: **Fundamental Science**

Industry: **NOT related to industrial**

Unavailable dates:

Laboratory support facility

- [ ] Simulation support (C-lab)
- [ ] SAXS support through PSB
- [ ] Containment level 2 biology lab
- [ ] Chemistry Labs
- [ ] MSSL
- [ ] PSCM lab
- [ ] EMBL lab

Instruments

Requested instrument	Days
D2B	**2**
D1B	**2**

Requested starting time

- [ ] 1. Jan/Feb
- [ ] 2. Mar/Apr
- [x] 3. May/Jun
- [x] 4. Jul/Aug
- [ ] 5. Sep/Oct
- [ ] 6. Nov/Dec

Comment: **11 temp x 4h /tempe= 44 h (D1B) and 3 temp 7h /temp= 21 h x 2 samples =42h (D2B)**

Sample availibility: **march-april**

Instruments' logical connection: **D2B AND D1B**

Experimental details

Energy/Wavelength range: **2.52 D1B, 1.594 D2B**

Resolution in energy or wavelength:

Range of momentum transfer:

Resolution in momentum transfer:

To be filled in by ILL

Sample environment code	Comments by Health Physics Officer and Safety Engineer
CO	

Abstract

Magnetic ionic liquids (MILs) are molten salts formed entirely of ions, which have a melting point below 100 ºC. The great variety of possible combinations of anions and cations makes them a huge potential field of development of smart materials with a primary focus in Materials Science; supported by the growing interest of chemists, physicists, and materials scientists. In the search of developing new MILs with enhanced magnetic response at room temperature, we have synthetized a new family based on imidazolium cation and [Fe2OX6]- anion. Therefore, in this proposal we ask for 2 days at D2B high resolution diffraction instrument to obtain accurate magnetic structure characterization and phase transition of two new MILs with formula Dimin[Fe2OX6]- (X = Cl and Br). The magnetic structure characterization of these AF compounds with polar space group will be carried out using D1B high flux and medium resolution diffractometer, for that we ask for two days of beam-time.

Sample description

Substance/Formula: **compounds based on (Î¼-Oxo)bis**

Mass (mg): **3** State: **powder**

Size (mm3): **1500 mm3**

Surface area (mm2):

Space group: **Fdd2**

Container: **cylinder**

Unit cell dimension:	a = **27.9248**	b = **22.5734**	c = **7.33031**
T(k)= **100 K**	α = **90**	β = **90**	γ = **90**

Solvent SLD:

Particle SLD:

Sample environment equipment (supplied by ILL)

Environment equipment: **standard orange**
cryostat 1.5 - 300 K

Laser: **None**

Use of gas: **None**

Temperature range: **1.8-300 K** Pressure range:

Magnetic field strength:

Danger associated with ancillary equipment: ☐ **Yes** ☐ **Uncertain** ☑ **No**

Safety aspects

No danger associated with this sample

Danger associated with the sample preparation:	☐ **Yes**	☐ **Uncertain**	☑ **No**
Danger associated with the sample handling:	☐ **Yes**	☐ **Uncertain**	☑ **No**

Type of waste to be processed after experiment: ☐ **Chemical** ☐ **Biological** ☐ **Nanoparticles** ☐ **Radioactive**

Publication

Multielectron oxidation in a ferromagnetically coupled dinickel(ii) triple mesocate, Ferrando-Soria J., Fabelo O., Castellano M., Cano J., Fordham S., Zhou H.C., Chemical Communications, (2015), 51, 13381-13384

A multifunctional magnetic material under pressure, Rodríguez-Velamazán J.A., Fabelo O., Beavers C.M., Natividad E., Evangelisti M., Roubeau O., Chemistry - A European Journal, (2014), 20, 7956-7961

Dryness sensitive porous 3d-4f metal-organic framework with unusual dynamic behaviour, Fabelo O., Cañadillas-Delgado L., Pasán J., Díaz-Gallifa P., Labrador A., Ruiz-Pérez C., CrystEngComm, (2012), 14, 765-767

Influence of the alkaline earth cations on the topology of MII/CuII mixed-metal¿organic frameworks (M = Ca, Sr and Ba), Ferrando-Soria J., Rood M.T.M., Julve M., Lloret F., Journaux Y., Pasán J., Ruiz-Pérez C., Fabelo O., Pardo E., CrystEngComm, (2012), 14, 761-764

Low Temperature Magnetic Ordering of the Magnetic Ionic Plastic Crystal, Choline[FeCl4], de Pedro I., Garcia-Saiz A., Andreica D., Barquin L., Fernandez-Diaz M., Blanco J., Amato A., Fernandez J., Journal of Physics: Conference Series, (2015), 663, 012012

Neutron Powder Diffraction study of the Magnetic Ionic Liquid Emim[FeCL4] and its deuterated phase, Garcia-Saiz A., de Pedro I., Barquin L., Fernandez-Diaz M., Blanco J., Fernandez J., Journal of Physics: Conference Series, (2015), 663, 012008

Anion¿¿ and Halide¿Halide Nonbonding Interactions in a New Ionic Liquid Based on Imidazolium Cation with Three-Dimensional Magnetic Ordering in the Solid State, Garcia-Saiz A., de Pedro I., Migowski P., Vallcorba O., Junquera J., Blanco J., Fabelo O., Sheptyakov D., Waerenborgh J., Fernandez-Diaz M., Rius J., Dupont J., González J., Fernandez J., Inorganic chemistry - Holleman A.F. /Wiberg E. - Academic Press - 1995 - 20.1/280, (2014), 53, 8384-8396

Magnetic ionic plastic crystal: choline[FeCl4], de Pedro I., Garcia-Saiz A., González J., Ruiz de Larramendi I., Rojo T., Afonso Carlos A. M., Simeonov Svilen P., Waerenborgh J. C., Blanco Jesús A., Ramajo B., Fernandez J. Rodríguez, Physical Chemistry Chemical Physics, (2013), 15, 12724

Ammonium-cobalt-nickel phosphates, NH4[Co1¿xNixPO4]·H2O, Torre-Fernández L., Trobajo C., de Pedro I., Alfonso B.F., Fabelo O., Blanco J.A., García J.R., García-Granda S., Journal of Solid State Chemistry, (2013), 206, 75-84

Magnetovolume and magnetocaloric effects in Er2Fe17, Alvarez-Alonso P., Gorria P., Blanco J.A., Sánchez-Marcos J., Cuello G.J., Puente-Orench I., Rodríguez-Velamazán J.A., Garbarino G., de Pedro I., Rodríguez Fernández J., Sánchez Llamazares J.L., Physical Review B, (2012), 86, 184411-1-184411-10

Sinusoidal magnetic structure in a three-dimensional antiferromagnetic Co2(OH)AsO4: Incommensurate-commensurate magnetic phase transition, de Pedro I., Rojo J.M., Rodríguez Fernández J., Fernández-Díaz M.T., Rojo T., Physical Review B, (2010), 81, 134431-1-134431-14

Max von Laue ¿ Hundred years of crystal diffraction, Fernández-Díaz M.T., Lemée-Cailleau M.H., Neutron News, (2013), 24, 11-12

Lithium distribution in aluminum-free cubic Li7La3Zr2O12, Xie H., Alonso J.A., Li Y., Fernández-Díaz M.T., Goodenough J.B., Chemistry of Materials, (2011), 23, 3587-3589

Magneto-structural correlations on new bimetallic-anionic paramagnetic ionic liquids with 3D magnetic ordering in its solid state.

Introduction: In recent years there has been a tremendous expansion in the design and synthesis of ionic liquids (ILs). Amoung them have highlighted the magnetic ionic liquids (MILs) fueled by the possibility of combining IL properties with additional intrinsic thermochromic,[1] magnetoelectrochromic[2] or luminescent[3] properties, depending on the paramagnetic ion used. The compositions of most MILs reported to date are based on a charge and molar ratio of 1:1, so that monocationic and monoanionic species are stoichiometrically paired. However, dicationic-containing ILs, generally as solids or with melting point near room temperature, can afford new supramolecular IL architectures with very interesting magnetic phenomena and potential applications ranging from magnetic hydraulics in engineering,[4] to esterification of oleic acid to biodiesel. [5]

Preliminary research and results: Recently we have investigated the magneto-structural properties of 4 different monocationic MILs, $A[FeCl_4]$ or $A[FeBr_4]$, being A an imidazolium-based counterion (Dimin: 1-3 dimethylimidazolium; or Edimim: 1-ethyl-3 methylimidazolium)[6-8]. Combining synchrotron powder X-ray and neutron diffraction we have determined their solid-solid phase transitions as well the magnetic structures. Our results reveal that i) halogen–halogen interactions are the main force inducing the 3D magnetic ordering in the solid state (ii) the spin population in the metal complex anion together with the distances and angles between the superexchange pathways [Fe–X/X–Fe(X = halide)] play a decisive role in attaining the 3D magnetic ordering and (iii) a less electronegative halide ion rises the efficiency of the magnetic couplings.

Actually, in the search of developing new MILs with enhanced magnetic response at room temperature, a new synthetic routes have been developed in our research group. The objective is to promote the clusterization of the Fe(III) ions in order to increase the magnetic interactions. Therefore, we have synthetized a new family of MILs based on imidazolium cation and $[Fe_2OX_6]^-$ anion, $DiminFe_2OX_6$ (X = Cl and Br). The compositions of these MILs are based on a charge and molar ratio of 1:1 of monocationic and bimetallic-anionic species, which are stoichiometrically paired. Thus, $DiminFe_2OX_6$ (X = Cl and Br) (X = Cl and Br) show a much larger effective magnetic moment [μ_{eff} = 8.35 and 7.90 μ_B for Cl (see figure 1) and Br, respectively] due to the doubled concentration of iron centers per mole. Consequently, it will be easier to tune their physicochemical properties in their liquid state by using external magnetic fields, which constitutes a fundamental step for their technological applications. In addition, at low

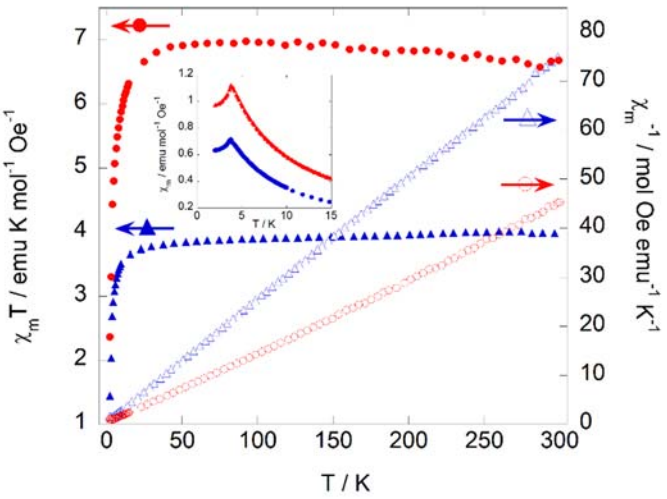

***Figure 1**. Comparative of the temperature dependence of $\chi_m T$ and $1/\chi_m$ for Dimim[$FeCl_4$] and the new dinuclear-based Dimim[Fe_2OCl_6] compound measured under 1kOe. The upper inset shows an enlargement of low temperature region of χ_m.*

temperatures, the magnetic susceptibility exhibit a 3D maximum at approximately 4.6 K and 8.2 K for DiminFe_2OCl_6 (see figure 1) and DiminFe_2OBr_6 respectively, revealing the existence of a new MILs family with three-dimensional magnetic ordering in the solid state.

Recently we have determined the crystal structure of the bromide compound by single crystal X-ray diffraction at low temperature (see Figure 2). The analysis of the data collected reveals that this MIL, crystallizes in a polar *Fdd*2 space group with a crystal structure that can be seen as layers of $[Dimim]^+$ cations and dinuclear $[Fe_2OBr_6]^-$ anions stacked along the *a*-direction. However, it is still necessary to determine from both, experimental and theoretical points of view, the magnetic self-assembly of the anion species in the crystal framework which drives the cooperative magnetic effects in these materials. A good understanding of these issues would allow an improvement of their technological applications.

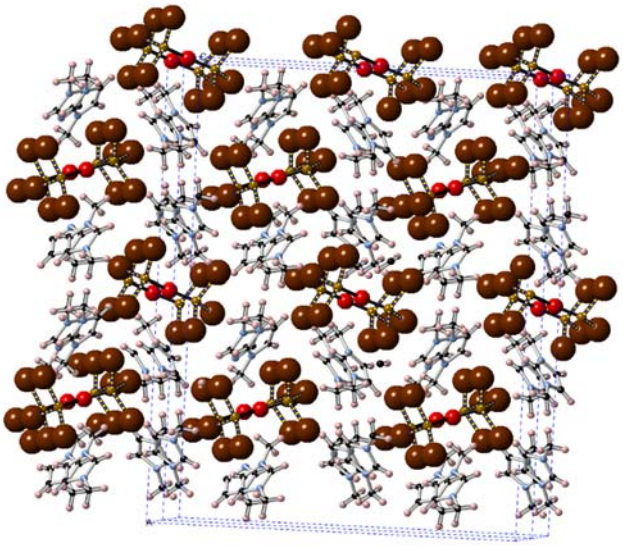

***Figure 2**. Crystal structure at 100 K of* Dimim[Fe_2OBr_6] *in the a,c projection obtained by single crystal experiments. Red (iron), brown (bromine), grey (carbon), blue (nitrogen) and white (hydrogen). The blue and green dashed squares represent the unit cells.*

Proposed experiments: The main objective of the proposed proposal is to determine the solid-solid phase transitions and the magneto-structural correlations of the Dimim[Fe_2OBr_6] and the Dimim[Fe_2OCl_6] . These results will be compared with the previous mononuclear MIL's. To carry out this task we need an accurate nuclear determination, involving the localization of the hydrogen atoms, which have been included in the preliminary X-ray structural model in the theoretical calculated positions. The determination of the magnetic structures of these MILs is the second objective of this proposal taking in account that the influence of the polar space group in the magnetic structure could give rise to complex magnetic structures.

We estimate that for these experiment, we need 2 days (3 temperatures× 7h /temperature = 21 h x 2 samples = 42 hours) and 2 days (11 temperatures× 4h /temperature= 44 h) of beam time on D2B and D1B respectively, to carry out neutron powder diffraction experiments with good statistics above and below the magnetic and structural transitions. These experiments will allow us to i) determine the crystal structure and phase diagram ii) resolve the magnetic structure and iii) follow the temperature dependence of the magnetic ordering exhibited by these new MILs. This work will be part of the Degree Project of Palmerina Gonzalez Izquierdo in the framework of the internships 2016 project.

References:

[1] Okuhata, M.; Funasako, Y.; Takahashi, K.; Mochida, T. *Chem. Comm.* **2013**, *49*, 7662. [2] Branco, A.; Branco, L. C.; Pina, F. *Chem. Comm.* **2011**, *47*, 2300.[3] Mallick, B.; Balke, B.; Felser, C.; Mudring, A.-V. *Angew. Chem. Int. Edit.* **2008**, *47*, 7635.[4] Scovazzo, P.; Portugal, C. A. M.; Rosatella, A. A.; Afonso, C. A. M.; Crespo, J. G. *J. Colloid. Interf. Sci.* **2014**, *428*, 16. [5] Anderson, J. L. *Anal. Chem.* **2015**, *87*, 1552. [6]García-Saiz A.; Migowski P.; Vallcorba O.; Junquera J., Blanco J. A.; González J. A.; Fernández-Díaz M. T.; Rius J.; Dupont J.; Rodríguez Fernández J.; de Pedro I. *Chem. Eur. J.*, **2014**, 20, 72. [7]García-Saiz A.; de Pedro I.; Migowski P.; Vallcorba O.; Junquera J.; Blanco J. A.; Fabelo O.; Sheptyakov D.; Waerenborgh J. C.; Fernández-Díaz M. T.; Rius J.; Gonzalez J. A.; Fernández J. R. *Inorg. Chem.*, **2014**, 53, 8384. [8] García-Saiz A.; de Pedro I.; Vallcorba, O.; Migowski, P.; Campo, I.; Barquin, L. F.; Abrahams I.; Motevalli M.; Dupont J.; Gonzalez J.A.; Fernández J. R. RSC Adv., **2015** ,5, 60835-60848.

Bibliography

[1] Jason P. Hallett and Tom Welton. Room-temperature ionic liquids: Solvents for synthesis and catalysis. *Chemical Reviews*, 111(5):3508–3576, 2011.

[2] Satoshi Hayashi and Hiro o Hamaguchi. Discovery of a magnetic ionic liquid [Bmim]$FeCl_4$. *Chemistry Letters*, 33:1590–1591, 2004.

[3] Masanari Okuno, Hiro o Hamaguchi, and Satoshi Hayashi. Magnetic manipulation of materials in a magnetic ionic liquid. *Applied Physics Letters*, 89, 2006.

[4] Esther Santos, Jonathan Albo, Andreia Rosatella, Carlos A.M. Afonso, and Ángel Irabien. Synthesis and characterization of magnetic ionic liquids (MILs) for CO_2 separation. *Journal of Chemical Technology and Biotechnology*, 89(6):866–871, jun 2014.

[5] P. Brown, A. Bushmelev, C. P. Butts, J. Cheng, J. Eastoe, I. Grillo, R. K. Heenan, and A. M. Schmidt. Magnetic control over liquid surface properties with responsive surfactants. *Angew. Chem. Int. Ed.*, 51:2414–2416, jan 2012.

[6] K. D. Clark, O. Nacham, T. Li H. Yu, M. M. Yamsek, D. R. Ronning, and J. L. Anderson. Extraction of DNA by magnetic ionic liquids: tunable solvents for rapid and selective DNA analysis. *Analytical Chemistry*, 87:1552–1599, 2015.

[7] A. H. Mohammad Fauzi, Amin, N. A. S., and R. Mat. Esterification of oleic acid to biodiesel using magnetic ionic liquid: Multi-objective optimization and kinetic study. *Applied Energy*, 114:809–818, feb 2014.

[8] Abel García-Saiz. *Propiedades magnéticas y estructurales de nuevos líquidos iónicos magnéticos (MILs) basados en imidazolio y haluros de hierro*. PhD thesis, Universidad de Cantabria, may 2016.

[9] Agustí Lledós, Marcial Moreno-Mañas, Mariona Sodupe, Adelina Vallribera, Ignasi Mata, Benjamín Martínez, and Elies Molins. Bent and linear forms of the (μ-oxo)bis[trichloroferrate(III)] dianion: An intermolecular effect structural, electronic and magnetic properties. *European Journal of Inorganic Chemistry*, (23):4187–4194, dec 2003.

[10] P. Carty, K. C. Clare, J. R. Creighton, E. Metcalfe, E. S. Raper, and H. M. Dawes. The preparation, crystal structure and thermal analysis of bis(ferrocenium)[μ_2-oxo bis(trichloroferrate(III))]. *Inorganica Chimica Acta*, 112:113–117, 1986.

[11] Eberhard W. Neuse, Fathima B.D. Khan, Klaus Berhalter, and Ulf Thewalt. Diammonium μ-oxobis[trichloroferrate(III)] salts. crystal and molecular structure of bis(benzyldimethylphenylammonium) μ-oxobis(trichloroferrate). *Journal of Crystallographic and Spectroscopic Research*, 16(4), 1986.

[12] Jui-Cheng Chang, Wen-Yueh Ho, I-Wen Sun, Yu-Kai Chou, Hsin-Hsiu Hsieh, Tzi-Yi Wu, and Shih-Shin Liang. Synthesis and properties of new (μ-oxo)bis[tricholoferrate(III)] dianion salts incorporated with dicationic moiety. *Polyhedron*, 29:2976–2984, 2010.

[13] Sara Busi, Manu Lahtinen, Reijo Sillanpää, and Kari Rissanen. A linear Fe-O-Fe unit in bis(dibenzyldimethylammonium) μ-oxobis[tribromoferrate(III)]. *Acta Crystallographica*, C62:m458–m460, 2006.

[14] Norah Maithufia and Stefanus Otto. The bis(acetonitrile-κn)bis[n,n-bis-(diphenylphosphanyl)ethanamine κ^2p,p']iron(II) tetrabromidoferrate(II) and I-oxido-bis[tribromidoferrate(III)] complex salts. *Acta Crystallographica*, C67:279–283, 2011.

[15] A. K. Abdul-Sada and K. R. Seddon and N. J. Stewart. Ionic liquids, `http://www.google.com/patents/WO1995021872A1?cl=en`.

[16] Abel García-Saiz, Imanol de Pedro, Pedro Migowski, Oriol Vallcorba, Javier Junquera, Jesús A. Blanco, Oscar Fabelo, Denis Sheptyakov, Joao Carlos Waerenborgh, María Teresa Fernández-Díaz, Jordi Rius, Jairton Dupont, Jesús Antonio Gonzalez, and Jesús Rodríguez Fernández. Anion-π and halide–halide nonbonding interactions in a new ionic liquid based on imidazolium cation with threedimensional magnetic ordering in the solid state. *Inorganic Chemistry*, 53:8384–8396, 2014.

[17] Abel García-Saiz, Pedro Migowski, Oriol Vallcorba, Javier Junquera, Jesús Angel Blanco, Jesús Antonio González, María Teresa Fernández-Díaz, Jordi Rius, Jairton Dupont, Jesús Rodríguez Fernández, and Imanol de Pedro. A magnetic ionic liquid based on tetrachloroferrate exhibits three-dimensional magnetic ordering: A combined experimental and theoretical study of the magnetic interaction mechanism. *Chemistry-A European Journal*, 20:72 – 76, 2014.

[18] Agilent Technologies UK Ltd. Agilent, CrysAlis PRO, 2011.

[19] George M. Sheldrick. A short history of SHELX. *Acta Crystallographica Section A*, 64:112–122, sep 2007.

[20] L. J. Farrugia. Wingx suite for small-molecule single-crystal crystallography. *Journal of Applied Crystallography*, 32:837–838, 1999.

[21] K Brandeburg and H. Putz GbR. DIAMOND 2.1d, Crystal Impact GbR, 2000.

[22] F. Moussa, M. Hennion, J. Rodríguez-Carvajal, L. Pinsard, and A. Revcolevschi. Spin waves in the antiferromagnet perovskite $LaMnO_3$: A neutron-scattering study. *Physical Review B*, 54(21):15149, dec 1996.

[23] K. S. Murray. Binuclear oxo-bridged iron(III) complexes. *Coordination Chemistry Reviews*, 12:1–35, 1974.

[24] N. N. Greenwood. *Spectroscopic Properties of Inorganic and Organometallic Compounds*, volume 8. The Chemical Society, Burlington House, London, W1V 0BN, 1974.

[25] R. M. Solbrig, IL. L. Duff, D. F. Shriver, and I. M. Iuotz. Raman and infrared spectroscopy of the oxo-bridged iron(III) complex, $[Cl_3Fe\text{-}O\text{-}FeCl_3]^{-2}$ as a spectroscopic model for the 0xo bridge in hemerythrin and ribonucleotide reductase. *Joumal of Inorganic Biochemistry*, 17:69–74, 1982.

[26] Tobias Bäcker, Oliver Breunig, Martin Valldor, Klaus Merz, Vera Vasylyeva†, and Anja-Verena Mudring. In-situ crystal growth and properties of the magnetic ionic liquid $[C_2mim][FeCl_4]$. *Crystal Growth Design*, 11(6):2564–2571, 2011.

[27] Olivier Khan. *Molecular Magnetism*. VCH Publishers, INC, 1993.

[28] Bhaskar Biswas, Merry Mitra, Jaydeep Adhikary, G. Rama Krishna, Partha Pratim Bag, C. Malla Reddy, Nuria Aliaga-Alcalde, Tanmay Chattopadhyay, Debasis Das, and Rajarshi Ghosh. Synthesis, x-ray structural and magnetic characterizations, and epoxidation activity of a new bis(μ-acetato)(μ-alkoxo) dinuclear iron(III) complex. *Polyhedron*, 53:264–268, 2013.